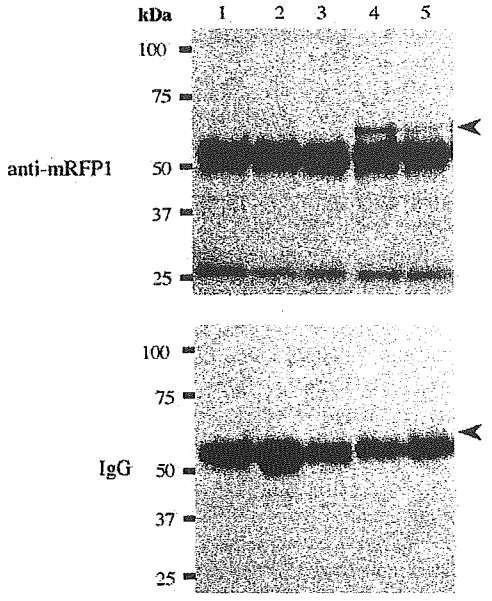

Fig. 5. Detection of complex formation between CPβ2-EGFP and mRFP1-CPα1 expressed in stable transformant Flp-In 293 cells by immunoprecipitation–immunoblot analysis. The transient expression of each fusion protein, CPβ2-EGFP or mRFP1-CPα1, in cells was performed using the plasmid for expression of the each fusion protein controlled by *EF-1α* promoter. The upper panel shows immunoblotting of the fusion protein using an anti-GFP antibody after immunoprecipitation with anti-mRFP1 antibody. The lower panel shows immunoblotting of the fusion proteins after immunoprecipitation with normal rabbit IgG. Lane 1 is mock-transfected Flp-In 293 cells, lane 2 is Flp-In 293 cells transiently transfected with pEXPR-*mRFP1-cpα1*, lane 3 is Flp-In 293 cells transiently transfected with pEXPR- *cpβ2-EGFP*, lane 4 is stably transformed Flp-In 293 cells carrying the *cyclin E/cpβ2* and *EF-1α/cpα1* transgenes and lane 5 is stably transformed Flp-In 293 cells carrying the *cyclin E/cpβ2* and *cdc2/cpα1* transgenes. The position of the band corresponding to each fusion protein CPβ2-EGFP is indicated by an arrowhead. The other interpretations and conditions are as in Fig. 1 and the experimental procedures.

When the *EF-1α* promoter was used to express these two cDNAs, the expression level of the downstream *cpα1*-cDNA was, in most cases, somewhat lower than that of the upstream *cpβ2*-cDNA (data not shown). This is not surprising since transcriptional interference has been reported to be frequently observed with closely apposed, independently regulated transcription units (Kadesch and Berg, 1986; Proudfoot, 1986). However, by inserting an insulator element HS4 (Chung et al., 1993; Hasegawa and Nakatsuji, 2002), at a site between *cpβ2*-cDNA and *cpα1*-cDNA, expression levels of the

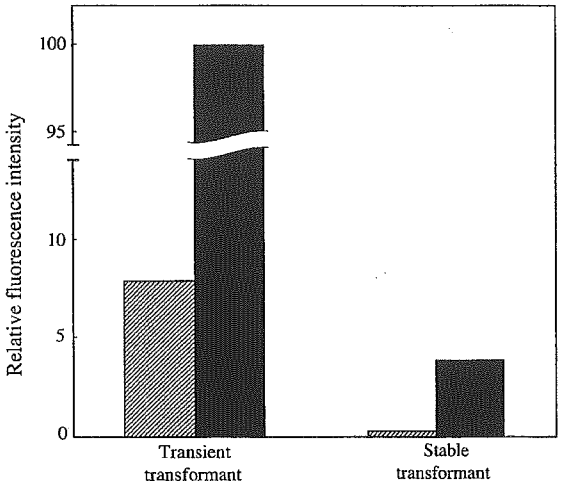

Fig. 6. Comparison of expression levels of the transgenes in stably transformed cells with those in transiently transformed cells. The relative fluorescence intensities measured with the images of Fig. 2 A-b and A-d and the images of Fig. 3 B-b and B-d are represented on the bars in the left (for the transgenes in the transiently transformed cells) and bars in the right (for the transgenes in the stably transformed cells), respectively. Shaded and closed bars represent the fluorescence intensities of EGFP and mRFP1, respectively.

downstream *cpα1*-cDNA was increased. The effect of the insulator elements on transcriptional interference with multiple cDNAs in a tandem structure on a single plasmid is under investigation (to be published). The interference effect is relatively weak when the promoter with low activity, such as *cyclin E*, is used for the upstream cDNA, as represented in this paper.

The expression levels of CPβ2-EGFP and mRFP1-CPα1 proteins in the stably transformed HeLa cells were lower than 4% of those levels observed with the transiently transformed cells harboring the comparable transgenes (Fig. 6). The system described above will enable controllable manipulation and visualization of physiological quantities of fluorescently labeled proteins in living cells and determination of their dynamic behavior, such as subcellular localization, functional protein complex formation and temporal protein–protein interactions.

Acknowledgements

The authors are grateful to Dr. Roger Tsien, UCSD (USA) for providing pRSET$_B$-mRFP1 and Dr. Yoshitake Nishimune and Dr. Hiromitsu Tanaka,

Osaka University (Japan) for valuable information in preparing CPα1 and CPβ2 constructs. This work has been supported in part by Grant-in-Aid for Scientific Research from the Ministry of Economy, Trade and Industry, Japan. Gateway®, Max Efficiency and Library Efficiency are registered trademarks of Invitrogen Corp. Clonase, pDONR, pEF5/FRT/V5-DEST, DH10B, DB3.1, pENTR, pEXPR, pDEST and Multisite are trademarks of Invitrogen Corp.

References

Barron-Casella, E.A., Torres, M.A., Scherer, S.W., Heng, H.H., Tsui, L.C., Casella, J.F., 1995. Sequence analysis and chromosomal localization of human Cap Z. Conserved residues within the actin-binding domain may link Cap Z to gelsolin/severin and profilin protein families. J. Biol. Chem. 270, 21472–21479.

Bernard, P., Kezdy, K.E., Van Melderen, L., Steyaert, J., Wyns, L., Pato, M.L., Higgins, P.N., Couturier, M., 1993. The F plasmid CcdB protein induces efficient ATP-dependent DNA cleavage by gyrase. J. Mol. Biol. 234, 534–541.

Boshart, M., Weber, F., Jahn, G., Dorsch-Hasler, K., Fleckenstein, B., Schaffner, W., 1985. A very strong enhancer is located upstream of an immediate early gene of human cytomegalovirus. Cell 41, 521–530.

Campbell, R.E., Tour, O., Palmer, A.E., Steinbach, P.A., Baird, G.S., Zacharias, D.A., Tsien, R.Y., 2002. A monomeric red fluorescent protein. Proc. Natl. Acad. Sci. U.S.A. 99, 7877–7882.

Chung, J.H., Whiteley, M., Felsenfeld, G., 1993. A 5′ element of the chicken beta-globin domain serves as an insulator in human erythroid cells and protects against position effect in Drosophila. Cell 74, 505–514.

Cormack, B.P., Valdivia, R.H., Falkow, S., 1996. FACS-optimized mutants of the green fluorescent protein (GFP). Gene 173, 33–38.

Feng, Y.Q., Seibler, J., Alami, R., Eisan, A., Westerman, K.A., Leboulch, P., Fiering, S., Bouhassira, E.E., 1999. Site-specific chromosomal integration in mammalian cells: highly efficient CRE recombinase-mediated cassette exchange. J. Mol. Biol. 292, 779–785.

Furukawa, Y., Terui, Y., Sakoe, K., Ohta, M., Saito, M., 1994. The role of cellular transcription factor E2F in the regulation of cdc2 mRNA expression and cell cycle control of human hematopoietic cells. J. Biol. Chem. 269, 26249–26258.

Hasegawa, K., Nakatsuji, N., 2002. Insulators prevent transcriptional interference between two promoters in a double gene construct for transgenesis. FEBS Lett. 520, 47–52.

Hwang, A., Maity, A., McKenna, W.G., Muschel, R.J., 1995. Cell cycle-dependent regulation of the *cyclin B1* promoter. J. Biol. Chem. 270, 28419–28424.

Kadesch, T., Berg, P., 1986. Effects of the position of the simian virus 40 enhancer on expression of multiple transcription units in a single plasmid. Mol. Cell. Biol. 6, 2593–2601.

Kim, D.W., Uetsuki, T., Kaziro, Y., Yamaguchi, N., Sugano, S., 1990. Use of the human elongation factor 1 alpha promoter as a versatile and efficient expression system. Gene 91, 217–223.

Kishine, H., Sugiyama, K., Hijikata, M., Kato, N., Takahashi, H., Noshi, T., Nio, Y., Hosaka, M., Miyanari, Y., Shimotohno, K., 2002. Subgenomic replicon derived from a cell line infected with the hepatitis C virus. Biochem. Biophys. Res. Commun. 293, 993–999.

Ohtani, K., DeGregori, J., Nevins, J.R., 1995. Regulation of the *cyclin E* gene by transcription factor E2F1. Proc. Natl. Acad. Sci. U.S.A. 92, 12146–12150.

Proudfoot, N.J., 1986. Transcriptional interference and termination between duplicated alpha-globin gene constructs suggests a novel mechanism for gene regulation. Nature 322, 562–565.

Sambrook, J., Russel, David, W., 2001. Molecular Cloning: A Laboratory Manual, third ed. Cold Spring Harbor Laboratory Press, Cold Spring Harbor, NY.

Schafer, D.A., Welch, M.D., Machesky, L.M., Bridgman, P.C., Meyer, S.M., Cooper, J.A., 1998. Visualization and molecular analysis of actin assembly in living cells. J. Cell. Biol. 143, 1919–1930.

Sone, T., Yahata, K., Sasaki, Y., Hotta, J., Kishine, H., Chesnut, J.D., Imamoto, F., 2005. Multi-gene gateway clone design for the expression of multiple heterologous genes in living cells: modular construction of multiple cDNA expression elements using recombinant cloning, doi:10.1016/j.jbiotec.2005.02.021.

Tanaka, M., Ueda, A., Kanamori, H., Ideguchi, H., Yang, J., Kitajima, S., Ishigatsubo, Y., 2002. Cell-cycle-dependent regulation of human *aurora A* transcription is mediated by periodic repression of E4TF1. J. Biol. Chem. 277, 10719–10726.

Villemure, J.F., Savard, N., Belmaaza, A., 2001. Promoter suppression in cultured mammalian cells can be blocked by the chicken beta-globin chromatin insulator 5′HS4 and matrix/scaffold attachment regions. J. Mol. Biol. 312, 963–974.

Xu, T., Rubin, G.M., 1993. Analysis of genetic mosaics in developing and adult Drosophila tissues. Development 117, 1223–1237.

Zhang, G., Gurtu, V., Kain, S.R., 1996. An enhanced green fluorescent protein allows sensitive detection of gene transfer in mammalian cells. Biochem. Biophys. Res. Commun. 227, 707–711.

MOLECULAR AND CELLULAR BIOLOGY, Aug. 2005, p. 7107–7119 Vol. 25, No. 16
0270-7306/05/$08.00+0 doi:10.1128/MCB.25.16.7107–7119.2005

HANP1/H1T2, a Novel Histone H1-Like Protein Involved in Nuclear Formation and Sperm Fertility

Hiromitsu Tanaka,[1] Naoko Iguchi,[1] Ayako Isotani,[2] Kouichi Kitamura,[1] Yoshiro Toyama,[3] Yasuhiro Matsuoka,[1] Masayoshi Onishi,[1] Kumiko Masai,[1] Mamiko Maekawa,[3] Kiyotaka Toshimori,[3] Masaru Okabe,[2] and Yoshitake Nishimune[1]*

Department of Science for Laboratory Animal Experimentation, Research Institute for Microbial Diseases,[1] Genome Information Research Center,[2] Osaka University, 3-1 Yamadaoka, Suita, Osaka 565-0871, and Department of Anatomy and Developmental Biology, Graduate School of Medicine, Chiba University, Chiba 260-8670,[3] Japan

Received 19 February 2005/Returned for modification 26 April 2005/Accepted 20 May 2005

We cloned a testis-specific cDNA from mice that encodes a histone H1-like, haploid germ cell-specific nuclear protein designated HANP1/H1T2. The HANP1/H1T2 protein was specifically localized to the nuclei of murine spermatids during differentiation steps 5 to 13 but not to the nuclei of mature sperm. HANP1/H1T2 contains an arginine-serine-rich domain and an ATP/GTP binding site, and it binds to DNA, ATP, and protamine. To investigate the physiological role of HANP1/H1T2, we generated *Hanp1/H1T2*-disrupted mutant mice. Homozygous *Hanp1/H1T2* mutant males were infertile, but females were fertile. Although a substantial number of sperm were recovered from the epididymides, their shape and function were abnormal. During sperm morphogenesis, the formation of nuclei was disturbed and protamine-1 and -2 were only weakly detectable in the nuclei. The chromatin packaging was aberrant, as demonstrated by electron microscopy and biochemical analysis. The mutant sperm exhibited deficient motility and were not competent to fertilize eggs under in vitro fertilization conditions; however, they were capable of fertilizing eggs via intracytoplasmic sperm injection that resulted in the birth of healthy progeny. Thus, we found that HANP1/H1T2 is essential for nuclear formation in functional spermatozoa and is specifically involved in the replacement of histones with protamines during spermiogenesis. At the time of submission of the manuscript, we found an independent publication by Martianov et al. (I. Martianov, S. Brancorsini, R. Catena, A. Gansmuller, N. Kotaja, M. Parvinen, P. Sassone-Corsi, and I. Davidson, Proc. Natl. Acad. Sci. USA 102:2808–2813, 2005) that reported similar results.

The complex process of spermatogenesis includes three major events: proliferation and differentiation of the spermatogonia, meiotic prophase in the spermatocytes, and drastic morphological changes during differentiation from the haploid round spermatids to the mature sperm (24). These events begin after birth, and approximately 35 days are required for the development of mature sperm in the mouse. The differentiation of the haploid germ cells (spermiogenesis) begins at 17 days of age in the mouse. Spermiogenesis involves diverse and complex processes, such as packaging and remodeling of the haploid germ cell nucleus, rearrangement of mitochondria, development of the flagellum, and formation of the acrosome. During this phase, the composition of the chromatin is altered dramatically (29). The changes in the nuclear proteins occur in association with the displacement of general nucleohistones by transition proteins (TNP) and other proteins, including a number of testis-specific histones and nonhistone chromosomal proteins (3, 12, 13, 17, 31) that are subsequently replaced with protamines to form nucleoprotamines (2, 20). The transition from histones to protamines in the chromatin of the haploid germ cells is accompanied by epigenetic changes (19) and the specific formation of nuclei in the sperm (25); these changes are associated with chromosome condensation and the shaping of the nucleus. Recently, mice with null mutations in TNP1 or TNP2 were found to be subfertile (32, 33), and mice with null mutations in both TNP1 and TNP2 were infertile (34). The nuclei of the sperm from the double TNP mutant mice contained protamines, despite the absence of an intermediate nucleosomal state involving TNPs (34).

Thus, the details of the mechanisms of these drastic physiological changes remain to be elucidated. Previously, we isolated cDNA clones of genes that are specifically expressed in mouse haploid germ cells from a subtraction library (9). In this study, we identified and characterized a novel haploid germ cell-specific nuclear protein (HANP1) in the mouse testis that is involved in the histone-protamine transition of sperm chromatin and the subsequent production of functional sperm.

MATERIALS AND METHODS

Cloning of the *Hanp1/H1T2* gene. A haploid germ-cell-specific cDNA library was previously generated in the pAP3neo vector by subtracting the mRNA from the testis of a 17-day-old mouse from a cDNA library produced from the testes of an adult (35-day-old) mouse (9). Clones were randomly selected from the subtracted cDNA library and used to probe Northern blots of testis-specific mRNA isolated from mice of various ages. We designated the testis-specific cDNA sequence tags as "transcripts increased in spermiogenesis" (TISP). One of the clones so isolated, TISP-8, possessed an open reading frame encoding a peptide with a high percentage of basic amino acids. Using the TISP-8 partial cDNA as a probe to screen an adult mouse testis library, we isolated the entire cDNA sequence, hereafter designated *Hanp1/H1T2*.

Biochemical characterization of HANP1/H1T2. Samples of various tissues were collected from C57BL/6 mice; the germ and somatic cells were prepared

* Corresponding author. Mailing address: Department of Science for Laboratory Animal Experimentation, Research Institute for Microbial Diseases, Osaka University, 3-1 Yamadaoka, Suita, Osaka 565-0871, Japan. Phone: 81-6-6879-8335. Fax: 81-6-6879-8339. E-mail: nishimun@biken.osaka-u.ac.jp.

from the testes as described in our previous report (16). The total RNAs were extracted from the samples using the RNAzol TM B reagent (Tel-Test Inc., Friendswood, TX) according to the manufacturer's instructions and were quantified by measurement of the optical density.

Synthetic peptides were designed from the deduced amino acid sequence of HANP1/H1T2 (ACH; EVRREISSHHEGKSTRLEKG; residues 71 to 90), synthesized, purified (SAWDY, Kyoto, Japan), and used to produce polyclonal antiserum to HANP1/H1T2 in rabbits.

Samples of various C57BL/6 mouse tissues were lysed with radioimmunoprecipitation assay buffer (10 mM Tris-HCl, pH 7.5; 0.15 M NaCl; 1% NP-40; 0.1% sodium deoxycholate; 0.1% sodium dodecyl sulfate [SDS]; 1 mM EDTA; 1 mM phenylmethylsulfonyl fluoride). Nuclear and cytoplasmic fractions of the testicular germ cells were prepared as described in our previous report (27). After centrifugation, aliquots of the samples (50 μg/lane) were separated by SDS–15% polyacrylamide gel electrophoresis (PAGE), and the proteins were transferred to polyvinylidene difluoride membranes (Millipore, Bedford, MA). The membranes were blocked with TBS-T (25 mM Tris-HCl, pH 7.5; 150 mM NaCl; 50 mM KCl; 0.05% Tween 20) containing 5% nonfat dried milk and then incubated with rabbit anti-HANP1/H1T2 polyclonal antibody diluted 1:1,500 in TBS (25 mM Tris-HCl, pH 7.5; 150 mM NaCl; 50 mM KCl). The membranes were then reacted with horseradish peroxidase-conjugated anti-rabbit immunoglobulin G, and the bound antibodies were detected using a peroxidase staining kit (Wako, Osaka, Japan).

The binding affinity between the HANP1/H1T2 protein and DNA or ATP was determined from the elution profile of HANP1/H1T2, protein from DNA-cellulose columns, or ATP-agarose beads. The nuclear lysate from testicular germ cells was applied to a DNA-cellulose column (Sigma-Aldrich, Tokyo, Japan) with a 0.5-ml bed volume in 50 mM Tris-HCl buffer (pH 7.5). After washing with 50 mM Tris-HCl buffer (pH 7.5), the column was eluted with various concentrations of NaCl, and each fraction was subjected to Western blotting with anti-HANP1/H1T2. To assess the binding affinity of HANP1/H1T2 for ATP, a plasmid encoding an enhanced green fluorescent protein (EGFP)-HANP1/H1T2 fusion protein was transfected into HEK-293 cells. Replicate samples of the transfected and mock-transfected cells were harvested 16 h later and lysed by homogenization in 1 ml of TBS-T buffer. After centrifugation, the cleared lysates were passed through 0.45-μm-pore-size SteraDisk filters (Kurabo, Osaka, Japan). The filtrates were mixed with ATP-agarose beads (Sigma-Aldrich) with a 0.5-ml bed volume in TBS-T buffer. The beads were washed three times with 0.5 ml of TBS-T buffer and eluted by boiling in 100 μl of SDS-PAGE sample buffer. The eluates (30 μl) were subjected to Western blot analysis using anti-GFP rat monoclonal antibodies.

The *Hanp1/H1T2*, *Prm1*, *hils1*, and *histone H1c* cDNAs were amplified by PCR and cloned into the EcoRI sites of the pmRFP-C1 and pEGFP-C1 plasmids (Clontech), respectively (13). The resulting clones expressed mRFP-HANP1/H1T2, EGFP-protamine, EGFP-HILS1, mRFP-HILS1, and EGFP-histone H1c fusion proteins and were used for coimmunoprecipitation experiments and for observation of subcellular localization in HEK-293 cells. The HEK-293 cells were transfected with the expression vectors using Lipofectamine Plus reagent (Life Technologies, Inc.).

DNA column chromatography of in vitro-translated HANP1/H1T2, histone H1, and HILS1 was performed to examine the DNA binding ability of each protein. PCR amplification of mouse histone H1 and *hils1* cDNA was performed with a set of synthetic oligonucleotide primers based on the histone H1c and *hils1* sequences (GenBank/EMBL/DDBJ accession numbers NM_015786 and AB022320 [13]). The *Hanp1/H1T2* cDNA fragment containing the entire coding region was amplified using PCR with the set of synthetic oligonucleotide primers Hanp1-5′ (5′-GGCCATGGCTGAGGCTGTCCAG-3′), based on the *Hanp1* sequence with a NcoI restriction site, and Hanp1-3′ (5′-GGCCATGGCATTAA GGAGACTCAGTGTCC-3′), also with an NcoI linker. Each PCR product was subcloned into the pET30a expression vector (Novagen) using appropriate restriction enzymes. For in vitro translation using STP2, T7 (Novagen) was used, and both proteins were labeled with ^{35}S-protein labeling mix (Amersham Biosciences), as described by the manufacturer. Aliquots of proteins translated in vitro were applied to double-stranded DNA-cellulose columns (Amersham Biosciences). After sufficient washing with the same buffer as that used for the DNA-binding assay, each column was eluted with five volumes of the same buffer containing seven consecutive concentrations of NaCl (0.1, 0.2, 0.3, 0.5, 1.0, 2.0, and 3.0 M) and denaturing buffer containing 6 M guanidine-HCl and 0.2 M acetic acid. The eluted samples were concentrated by trichloroacetic acid precipitation, and equal fractionation aliquots were subjected to SDS–15% PAGE. The gels were then fixed in a solution of 10% acetic acid with 10% methanol, dried, and autoradiographed using an ImageAnalyzer (Fuji Photo Film).

Construction of the *Hanp1/H1T2* targeting vector and production of *Hanp1/H1T2* knockout mice. The *Hanp1/H1T2*-targeting construct was created by PCR amplification of 5′ and 3′ homology arms of 3.5 and 4.9 kb, respectively, from 129Sv genomic DNA. The oligo primers used for amplification of the homology arms were designed to incorporate synthetic restriction enzyme sites at both ends. The two amplified fragments were digested with the appropriate enzymes and sequentially ligated into the polylinker cloning sites on either side of the neomycin resistance gene in the targeting vector backbone. The targeting vector construct contained the neomycin resistance gene and the thymidine kinase gene, both under the control of the phosphoglycerate kinase promoter. The vector plasmid was linearized by digestion with NotI prior to electroporation into W9.5 embryonic stem (ES) cells. Of the 720 G418-ganciclovir-resistant clones obtained, 4 were found by Southern blot analysis to have undergone the correct homologous recombination. The ES cells from each of the four lines were injected into C57BL/6J blastocysts, resulting in the birth of male chimeric mice. Highly chimeric males were mated with C57BL/6J wild-type females to generate F1 offspring, half of which were heterozygous for the targeted allele. Of the four ES cell lines injected, only one produced a high percentage of germ line chimeras. Heterozygous F_1 males were then crossed to C57BL/6 females to obtain heterozygous F_2 animals. Heterozygous F_2 animals were bred to obtain homozygous mutants and to verify the Mendelian pattern of inheritance. Ten mice older than 3 months of age were used to determine the fertility rate by monitoring three pregnancies in each fertile mouse. The assessment of phenotypic variation and the biochemical analyses were conducted on samples from at least three individuals, as described below.

Morphological assessment of testis and epididymal sperm. For immunohistochemical observation of HANP1/H1T2 expression, testes were collected from knockout and control mice, fixed in Carnoy's fixative, embedded in paraffin, and sectioned at a thickness of 8 μm. Sperm from the cauda epididymis were harvested, dried on glass slides, and fixed in Carnoy's fixative for 10 min. The samples were treated with 0.05 M β-mercaptoethanol in TBS before incubation with the appropriate monoclonal antibodies, as previously described (26, 34). For electron microscopic observations, the animals were perfused with 3% glutaraldehyde in HEPES buffer (10 mM HEPES, 145 mM NaCl). After fixation with 1% osmium tetroxide, the testes and cauda epididymides were embedded in Epon resin. Selected areas were sectioned and examined.

Analysis of sperm. The germ cell fractions were prepared from the testes as described in our previous report (16). The nuclei of germ cells and sperm were prepared by sonication, and the basic proteins were extracted and separated by PAGE on acid-urea gels (33). The fractions from three mice were loaded in duplicate on each of two acid-urea gels. One gel was stained with Coomassie brilliant blue to identify the nuclear proteins, and the other was used for Western blot analysis.

Fluorescence-activated cell sorting (FACS) analysis was performed to determine the extent of DNA condensation in sperm from the *Hanp1/H1T2* mutant mice, as previously described (33). Sperm were isolated from the cauda epididymides of mutant and control mice. After incubation for 1 h in TYH medium (30), the sperm were subjected to mild sonication and azide was added to a final concentration of 0.025%. The sperm were then stained with propidium iodide and analyzed on a flow cytometer.

Computer-assisted sperm analysis was performed to examine sperm motility, as previously described (28). At least 200 sperm were counted in order to evaluate the percentage of progressively motile sperm, the straight-line velocity, the curvilinear velocity (VCL), the amplitude of lateral head displacement, and linearity. Only the VCL data were reported.

In vitro fertilization assays were performed as previously described (30). Briefly, sperm samples were collected from the cauda epididymides of each male, capacitated in TYH medium at 37°C for 1 h, and then introduced into oocytes with cumulus cells. The inseminated oocytes were placed in 0.3 ml of TYH droplets, covered with mineral oil, and incubated at 37°C in 5% CO_2. After 24 h, successfully fertilized eggs were counted and transplanted into the uteri of pseudopregnant females.

Intracytoplasmic sperm injection (ICSI) was performed as described by others (15). Briefly, sperm collected from the epididymides were suspended in 12% polyvinylpyrolidone (360 kDa) and decapitated with one Piezo pulse (Prime Tech, Tokyo, Japan). The detached heads were introduced into the cytoplasm of unfertilized cumulus-free eggs. After incubation in kSOM medium for 24 h (11), the eggs, at the two-cell stage, were implanted into pseudopregnant females.

RESULTS

The testis-specific *Hanp1/H1T2* gene encodes a histone H1-like protein. To provide molecular tools for the examination of the processes involved in sperm morphogenesis, we had pre-

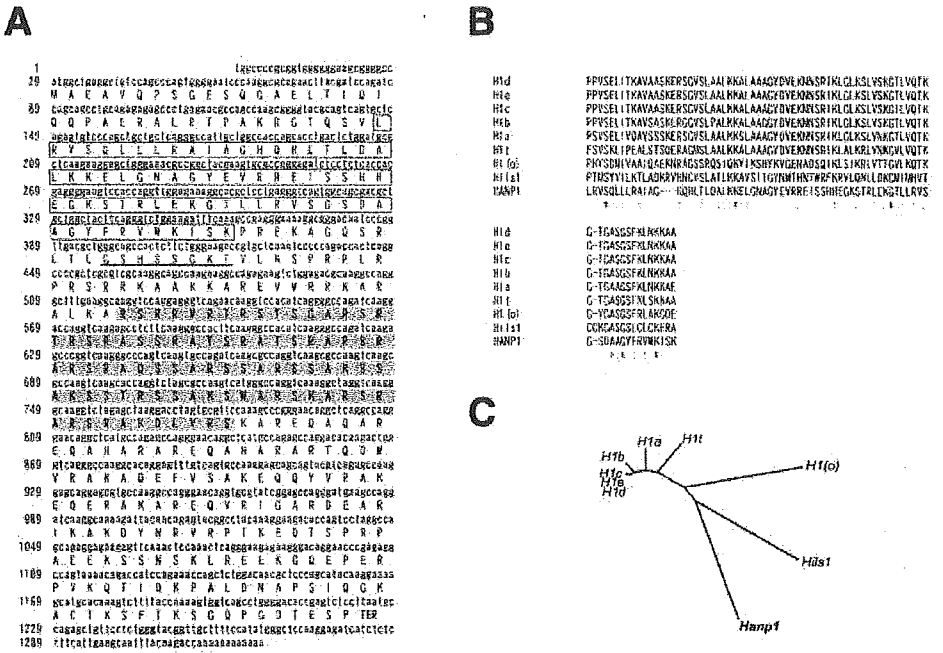

FIG. 1. Sequence analyses of the *Hanp1/H1T2* gene. (A) The full-length sequence of the *Hanp1/H1T2* cDNA (DNA Data Base of Japan, accession numbers AB016273 and AY496853). The box, bar, and shadowed box indicate the putative histone globular domain, ATP-binding site, and RS domain, respectively. (B) The alignment of the deduced amino acid sequence of the globular domain of HANP1/H1T2 with various histone H1 protein sequences. The asterisks and dots indicate similar and homologous amino acids, respectively. (C) A phylogenetic tree of the globular domains of various histone H1 proteins generated using the neighbor-joining method.

viously isolated many cDNA clones that are specifically expressed in testicular germ cells from a subtracted cDNA library produced using haploid germ cell-specific cDNA clones (9). In this study, we found that one clone, designated TISP-8 for transcript increased in spermiogenesis (TISP), encoded a protein containing an extensive series of basic amino acids. Using the TISP-8 partial cDNA as a probe, we isolated a complete cDNA clone, subsequently designated *Hanp1/H1T2*, from an

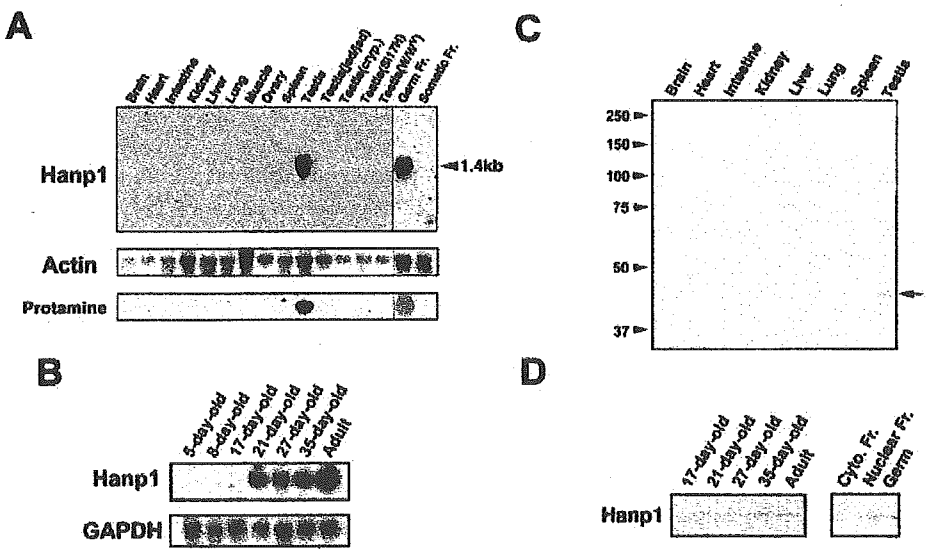

FIG. 2. The expression profiles of *Hanp1/H1T2* mRNA (A and B) and protein (C and D) in mouse tissues. (A) Total RNA was prepared from various organs and hybridized with a *Hanp1/H1T2*-specific probe. Cells recovered from adult mouse testes were separated into germ and somatic cell fractions. (B) The expression of *Hanp1/H1T2* mRNA in the testes at different stages of development (numbers indicate days of age). Western blot analysis of HANP1/H1T2 expression using anti-HANP1/H1T2 rabbit antiserum in various adult mouse tissues (C) and in the testes at different stages of development and in subcellular fractions of testicular germ cells (D). The cryptorchid (cryp.) testes and mutant testes of *jsd/jsd W/Wv S117H/S117H* mice do not have spermatocytes and more differentiated germ cells after 12 weeks of age. Fr., fraction.

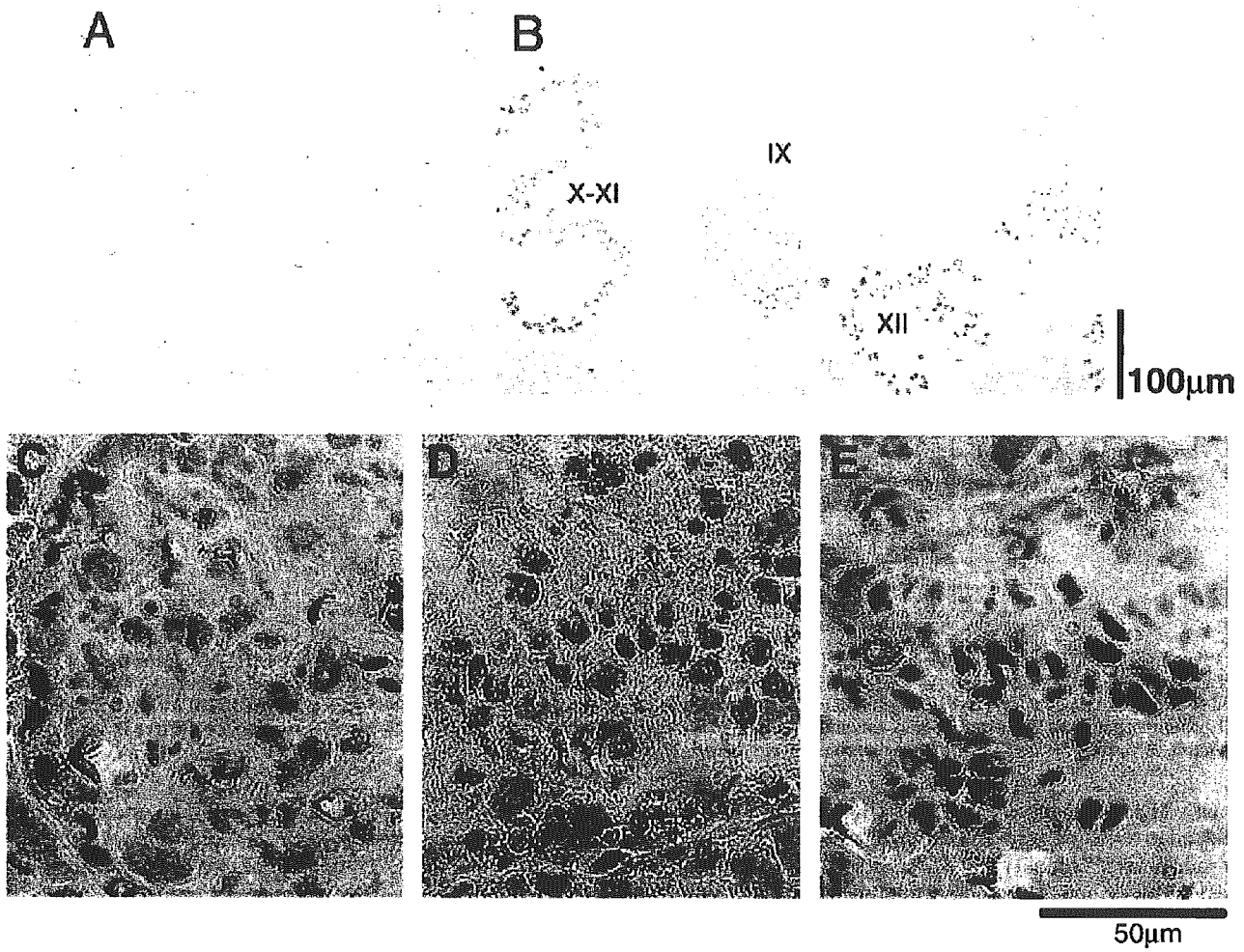

FIG. 3. Expression of HANP1/H1T2 in cross sections of the mouse testis. Immunohistochemical staining of testis tissue sections with preimmune serum (A) or anti-HANP1/H1T2 rabbit serum (B to E). Expression of HANP1/H1T2 during developmental stages V and VI (C), IX (D), and X and XI (E) of the seminiferous tubules. Higher magnification images of each stage were counterstained with hematoxylin (blue). The nuclei of round and elongated spermatids were strongly stained with anti-HANP1/H1T2 antibody (brown).

adult mouse testis library. The complete *Hanp1/H1T2* nucleotide sequence (DNA Data Bank of Japan, accession number AB016273), and the deduced amino acid sequence are shown in Fig. 1. The deduced amino acid sequence of the HANP1/H1T2 protein consisted of a region homologous to histone H1, an ATP/GTP-binding site motif A, an RS domain consisting of arginine-serine repeats, and 14 phosphorylation sites for protein kinase C (consensus sequence, S/T-X-R/K). The basic amino acids lysine and arginine composed 25% of the total amino acids predicted from the *Hanp1/H1T2* cDNA sequence (Fig. 1). Phylogenetic analysis of HANP1/H1T2 and the globular domains of histone H1 showed that HANP1/H1T2 probably shares a common ancestor with various histone H1s (Fig. 1C) and that it is conserved in the human (data not shown).

***Hanp1/H1T2* is specifically expressed in haploid germ cells.** Tissue-specific Northern blot analysis had previously shown that *Hanp1/H1T2* mRNA was exclusively expressed as a 1.4-kb transcript in the adult mouse testis but not in the testes of younger animals, in cryptorchid mice, or in mutants having no differentiated germ cells (7). In testicular cells, the expression of *Hanp1/H1T2* mRNA was not detected in somatic cells and was limited to germ cells (Fig. 2A) in animals older than 21 days of age (Fig. 2B), indicating that the positive cells were likely to be spermatids. Western blot analysis using anti-HANP1/H1T2 antiserum detected a 44-kDa band in the testes of mice older than 21 days (Fig. 2D) but showed no positive bands in sperm (data not shown). The HANP1/H1T2 protein was exclusively detected in the nuclear fraction (Fig. 2C and D) in Western blot analysis of subcellular extracts from testicular germ cells.

***Hanp1/H1T2* expression is localized to the nucleus.** The development of mouse haploid spermatids has been classified into 16 sequential steps following meiotic division (24). The immunohistochemical examination of the adult mouse testis showed that the nuclei of spermatids in developmental steps 5 to 13 were positive for HANP1/H1T2 (Fig. 3), which was consistent with the findings from the Western blots of adolescent testes and subcellular germ cell fractions (Fig. 2D). These

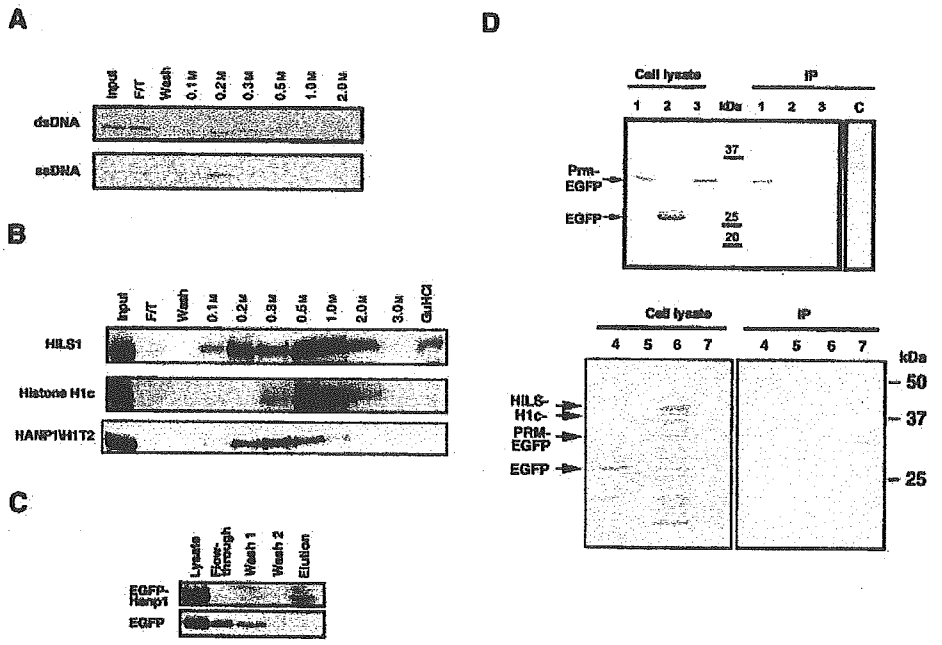

FIG. 4. Biochemical characterization of HANP1/H1T2 protein. (A) DNA binding assay with double-stranded (ds) or single-stranded (ss) DNA-cellulose columns. The chromatography conditions are indicated at the top. Input, the amount of HANP1/H1T2 applied to each column; F/T, flowthrough; Wash, wash fraction; numbers indicate the concentrations of NaCl in the elution buffer. The total protein contained in each fraction was electrophoresed, and Western blots were performed using anti-HANP1/H1T2 antiserum. (B) In vitro-translated and ^{35}S-labeled HANP1/H1T2, Hils1, or histone H1c protein was applied to a double-stranded DNA cellulose minicolumn and eluted with increasing concentrations of NaCl. Aliquots (wash and 0.1 to 3.0 M NaCl were 1/4 volume; the GuHCl was 1/12 volume) of each fraction were separated by SDS-PAGE, and the gels were autoradiographed. F/T and GuHCl represent the flowthrough fraction and denaturing buffer, respectively (13). (C) ATP binding assay on ATP-Sepharose columns. EGFP or EGFP-HANP1/H1T2 recombinant protein was applied to ATP-Sepharose affinity columns and washed with TBS-T buffer (wash fractions 1 and 2). The ATP-Sepharose was eluted by boiling in SDS-PAGE sample buffer, and Western blots were performed using anti-EGFP rat monoclonal antibody. (D) Coimmunoprecipitation of recombinant proteins mRFP-HANP1/H1T2 EGFP–protamine-1, EGFP-histone H1, and EGFP-HILS1. Recombinant proteins were coexpressed in HEK293 cells and electrophoresed (cell lysate) or coimmunoprecipitated with anti-mRFP rabbit serum and protein A-Sepharose beads (IP). Lane 1, EGFP–protamine-1 and mRFP-HANP1/H1T2; lanes 2 and 4, EGFP control and mRFP-HANP1/H1T2; lanes 3 and 7, EGFP–protamine-1 and mRFP control; lane 5, EGFP-histone H1 and mRFP-HANP1/H1T2; lane 6, EGFP-HILS1 and mRFP-HANP1/H1T2; lane C, EGFP–protamine-1 and mRFP-HILS1. Western blots were conducted using anti-EGFP rat monoclonal antibody. Numbers in the center of the panel indicate molecular mass markers (kilodaltons).

results indicated that the HANP1/H1T2 protein is localized to the spermatid nuclei and that the timing of *Hanp1/H1T2* gene transcription and translation is precisely regulated during the development of male germ cells.

HANP1/H1T2 is able to directly or indirectly bind to DNA, ATP, and protamines. The nuclear localization and elevated basic amino acid content of HANP1/H1T2 suggested an association of HANP1/H1T2 protein with nucleic acids. To examine the DNA binding activity of endogenous HANP1/H1T2 protein in male germ cells, testicular extracts were applied to double- or single-stranded calf thymus DNA-cellulose minicolumns, and the proteins were eluted with stepwise increasing concentrations of NaCl. HANP1/H1T2 was detected mainly in the fractions eluted from both types of DNA columns with 0.1 to 0.3 M NaCl (Fig. 4A), indicating that HANP1/H1T2 or its complexes bind to both double- and single-stranded DNA.

HANP1/H1T2 was also detected in the flowthrough fraction. The reapplication of the flowthrough fraction to fresh DNA-cellulose minicolumns showed the HANP1/H1T2 present in the flowthrough fraction rarely binds to the DNA columns (data not shown). Next, we compared the DNA binding ability with other linker histones expressed in spermiogenesis. HANP1 ability is weaker than both histone H1 and *hils1* (Fig. 4B). These results indicated that HANP1/H1T2 or its complexes might have alternative forms that are unable to bind to DNA. HANP1/H1T2 protein was also found to bind to ATP-agarose minicolumns, suggesting that ATP might act as a cofactor in the regulation of HANP1/H1T2 (Fig. 4C). We also examined the ATPase activity of mRFP-HANP1/H1T2 recombinant protein. However, we did not detect activity in the immunoprecipitant of an extract of HEK 293 cells expressing mRFP-HANP1/H1T2 (data not shown). HANP1/H1T2 was identified for the first time as a histone H1-like protein having an RS domain that is transiently expressed during mouse spermiogenesis.

Members of the SR protein family having RS domains play important roles in the tissue-specific regulation of alternative pre-mRNA splicing (10). Recently, it was also reported that RS domains were involved in protein-protein interactions (22). As HANP1/H1T2 is expressed in nuclei at the time of the transition from histones to protamines in chromatin during spermiogenesis, we examined whether HANP1/H1T2 associates with protamine-1 by using ectopic expression of tagged proteins, because neither the anti-HANP1/H1T2 nor anti-pro-

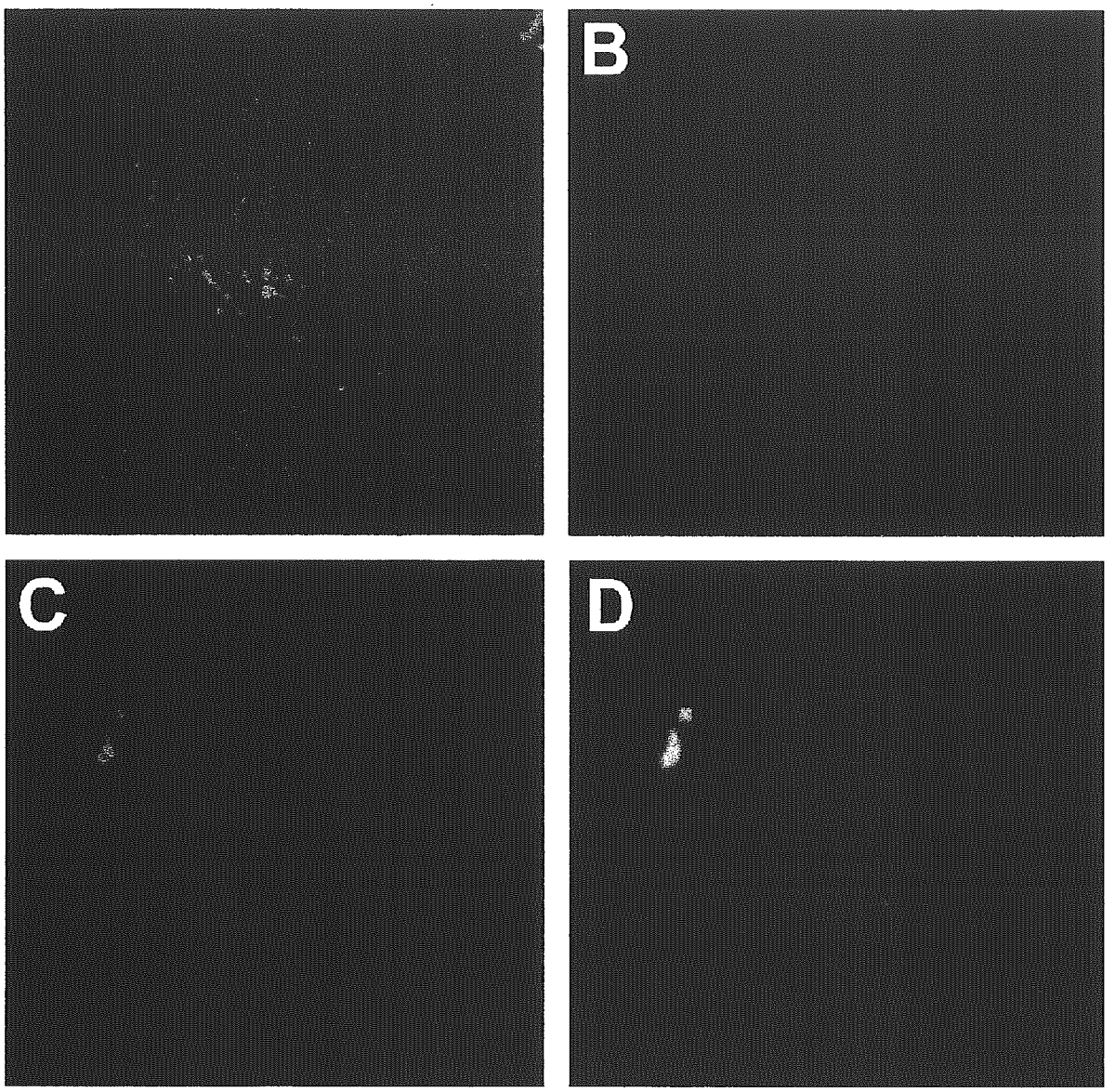

FIG. 5. Ectopic coexpression of mRFP-HANP1/H1T2 and EGFP-protamine fusion proteins in transfected cultured cells. HEK-293 cells were cotransfected with the expression vectors pmRFP-*Hanp1/H1T2* and pEGFP-Prm using Lipofectamine Plus reagent. The cells were observed 24 h after transfection using a Leica inverted fluorescence microscope under normal light (A) and with Leica fluorescein isothiocyanate filter sets for observation of the expression of mRFP (B) and GFP (C). (D) Merged image of mRFP and GFP fluorescence. Bar = 50 μm.

tamine antibody could be used for coprecipitation experiments. The coprecipitation of extracts of HEK 293 cells expressing both mRFP-HANP1/H1T2 and EGFP-protamine recombinant proteins indicated that HANP1/H1T2 associates with protamine either directly or indirectly (Fig. 4D). mRFP-HANP1/H1T2 did not associate with EGFP-*hils1* or histone H1, and mRFP-*hils1* did not associate with EGFP-protamine as a control (Fig. 4D). Figure 5 also shows that the recombinant EGFP–protamine-1 and mRFP-HANP1/H1T2 proteins were colocalized in the nuclei of HEK 293 cells and that these proteins were restricted to subnuclear foci within the nucleus. These results indicate that HANP1/H1T2 is able to associate with protamines.

Male *Hanp1/H1T2* null mice are infertile. To investigate the physiological role of HANP1/H1T2, we generated homozygous *Hanp1/H1T2* knockout mice. Homologous recombination was used to generate embryonic stem cell clones that were heterozygous for the *Hanp1/H1T2* mutation. To produce chimeric mice, the transgenic ES cells were injected into blastocysts that were subsequently implanted into pseudopregnant mice. The strategies used to produce the *Hanp1/H1T2* knockout mice and the Southern blot analysis of the mutant mice are shown in Fig. 6A and B. Crosses of heterozygous mutant pairs produced the expected ratio of wild-type, heterozygous, and homozygous genotype offspring, according to the classical Mendelian inheritance pattern. The body weights, growth rates of newborn

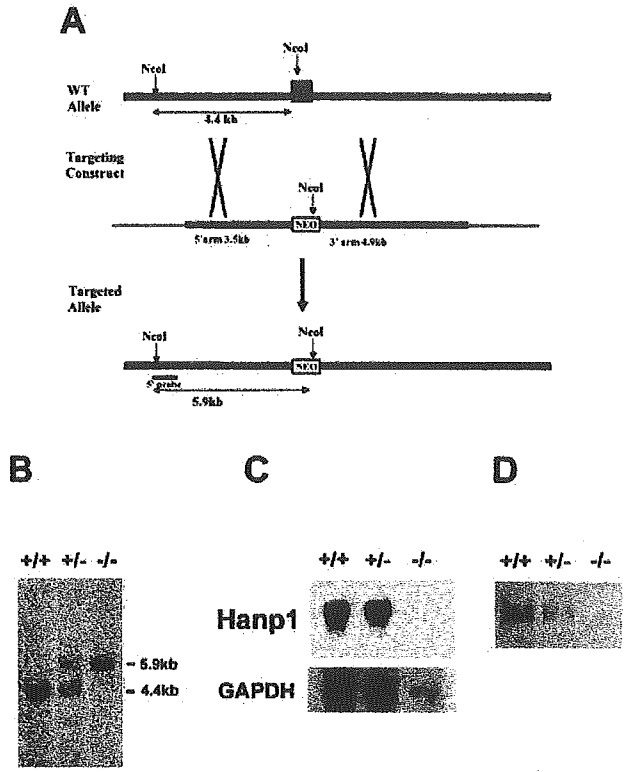

FIG. 6. *Hanp1/H1T2* gene targeting, identification, and expression of *Hanp1/H1T2* in gene-targeted mice. (A) Schematic representation of the strategy used for targeting the *Hanp1/H1T2* gene. The black box indicates the intronless *Hanp1/H1T2* gene. NcoI indicates the restriction enzyme recognition site. The gene targeting construct contained the neo gene (NEO in open box) placed between the 3.5-kb 5′ and the 4.9-kb 3′ homology arms. The thick and thin lines indicate the genomic and targeting vector DNA, respectively. (B) The targeted allele was identified by Southern blot analysis of NcoI-digested genomic DNA using a probe derived from the 5′ fragment of the vector. (C) Northern blot analysis. Transcripts of the *Hanp1/H1T2* gene were not detectable in the testes of homozygous *Hanp1/H1T2* knockout mice. The same filter was then rehybridized with a GAPDH cDNA probe as a control. (D) Western blot analysis of testicular lysates from adult mice using anti-HANP1/H1T2 antiserum. The HANP1/H1T2 protein was not detected in the testicular lysate of the homozygous *Hanp1/H1T2* knockout mouse. WT, wild type.

pups, and weights of various organs, including the testes and seminal vesicles of adult *Hanp1/H1T2* mutant mice, were not significantly different from those of wild-type mice. *Hanp1/H1T2* mRNA was not detectable by Northern blot analysis (Fig. 6C), and the 44-kDa HANP1/H1T2 protein was not detected on Western blots (Fig. 6D) of the testes of homozygous *Hanp1/H1T2* knockout mice. Microscopic examination of the testes did not show any significant differences among homozygous, heterozygous, and wild-type mice, but only homozygous *Hanp1/H1T2* male mutants were infertile. Matings between homozygous *Hanp1/H1T2* knockout males and wild-type females did not produce any successful pregnancies during more than 3 months of continuous cohabitation, even though many vaginal plugs were observed in the paired wild-type females (Table 1). The heterozygous male *Hanp1/H1T2* mutant mice and the homozygous females were all fertile and produced as many progeny per pregnancy as did their wild-type littermates.

TABLE 1. Fertility rate of mutant mice

Genotype	Male fertility[a]	Litter size[b]	Female fertility[c]	Litter size
+/+	10/10	8.1	10/10	8.4
+/−	10/10	8.6	10/10	9.0
−/−	0/10	0	10/10	8.4

[a] Number of fertile females per number of vaginal plugs.
[b] Average number of newborn pups.
[c] Wild-type males were mated with females of each genotype.

TABLE 2. Motility characteristics and in vitro fertilization of sperm from Hanp1-deficient mice

Genotype	*n*	Sperm no. (10^6)[a]	Motility (%)[b]	VCL	IVF
+/−	3	87 ± 7.5	93.0 ± 3.5	247.2 ± 10.3	98.8 ± 16.0
−/−	3	69 ± 16.0	23.7 ± 17.9*	148.8 ± 52.4*	0.0

[a] Number of sperm recovered from a cauda epididymis
[b] Motility (%) and curvilinear velocity (VCL) were measured after 1 h of incubation by computer-assisted sperm analysis. *, Statistically significant difference ($P < 0.01$).

***Hanp1/H1T2* knockout mice have defects in sperm nuclear formation.** Although similar numbers of sperm were recovered from the cauda epididymides of homozygous and heterozygous *Hanp1/H1T2* mutant males (Table 2), light microscopy showed that most of the sperm from homozygous *Hanp1/H1T2* mutants had abnormal kinks in the tails and abnormally shaped heads (Fig. 7a). Electron microscopy demonstrated that the step 6 spermatids from homozygous *Hanp1/H1T2* mutants exhibited nuclear abnormalities (Fig. 7b); the nuclear membranes were undulated, and the nuclei were invaginated. A clear halo was observed inside the nuclear membrane in mature spermatids (Fig. 7c) and epididymal sperm (Fig. 7d), apparently attributable to the condensed chromatin leaving an almost electron-transparent space near the nuclear membrane. These nuclear abnormalities were observed in cells at a stage of development in which HANP1/H1T2 expression normally occurs. Other observed abnormalities included dislocated necks of epididymal sperm (Fig. 7d); abnormalities in the heads of mature spermatids and sperm, such as remnants of the cytoplasm around the nucleus; and deformation and some vacuolation of the acrosomes (Fig. 7d). These abnormalities were found in germ cells that had differentiated beyond step 5, and no morphological abnormalities were found in earlier steps of spermiogenesis. Taken together, these findings indicate that the absence of HANP1/H1T2 expression leads to abnormalities in the formation of the spermatid nucleus, which in turn results in abnormal morphogenesis of other parts of the sperm, including the formation of kinks in the tails (14). Alternatively, the HANP1/H1T2 protein may directly affect various aspects of sperm morphogenesis.

***Hanp1/H1T2* mutant sperm exhibit abnormal movement.** As the morphological abnormalities described above appeared likely to cause motility defects in the mutant sperm, we performed computer-assisted sperm analysis to quantify the sperm motility after 1, 3, and 6 h of incubation in TYH medium (28). Table 2 shows the percent motility and the curvilinear velocity

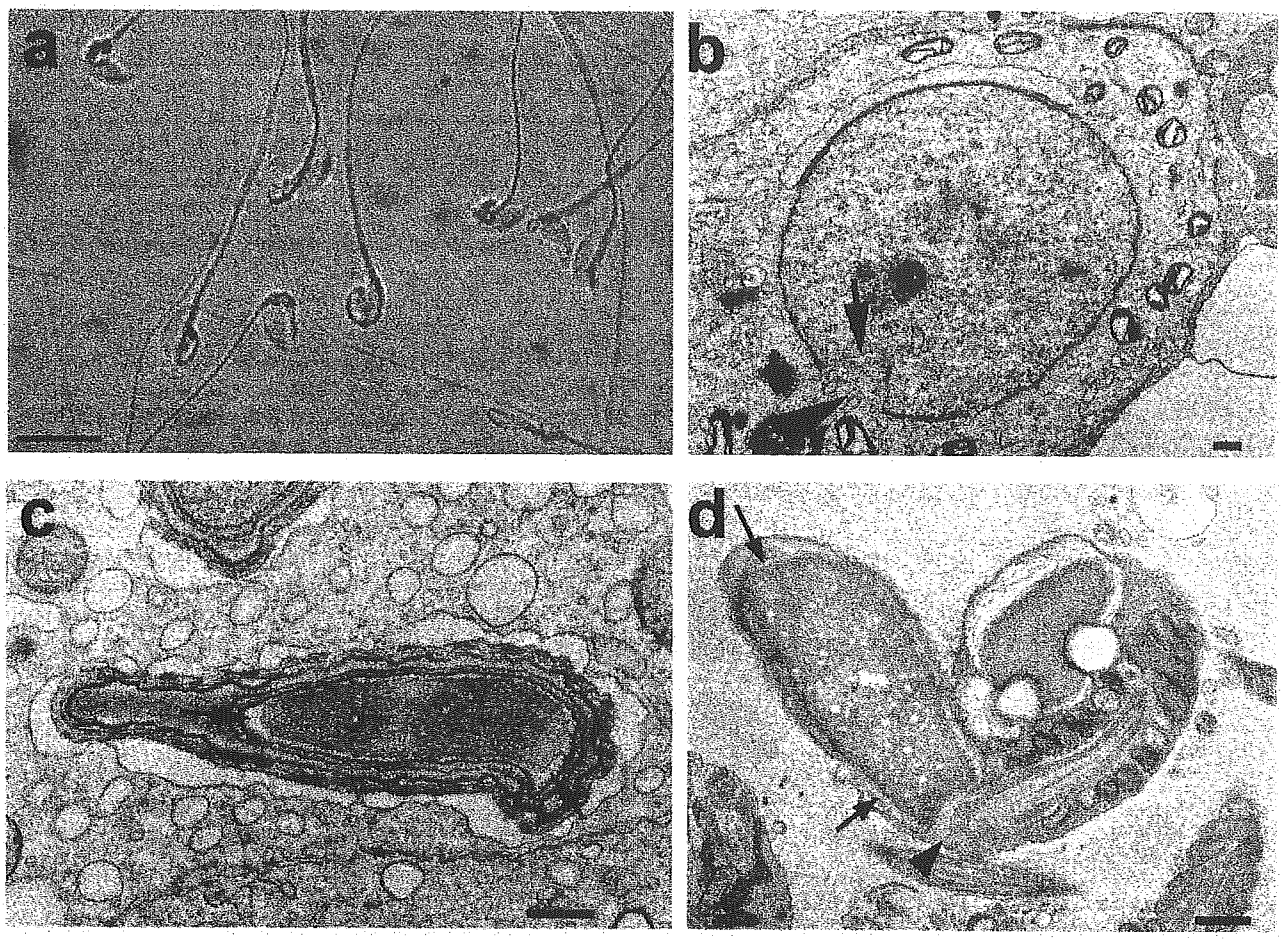

FIG. 7. Morphology of spermatids and sperm from homozygous *Hanp1/H1T2* mutant mice. (a) Light micrograph of cauda epididymal sperm. The mutant sperm have abnormal connections between the head and the neck. Bar = 10 μm. (b) Electron micrograph of a step 6 spermatid. The nuclear membrane is ruffled (arrow), and invagination of the nucleus is visible (arrowhead). Bar = 0.5 μm. (c) A step 12 spermatid. A pale halo can be observed under the nuclear membrane (arrows). Bar = 0.5 μm. (d) Sperm in the cauda epididymis. The arrows indicate a clear halo under the nuclear membrane. The sperm neck appears dislocated from the base of the head (arrowhead). Bar = 0.5 μm.

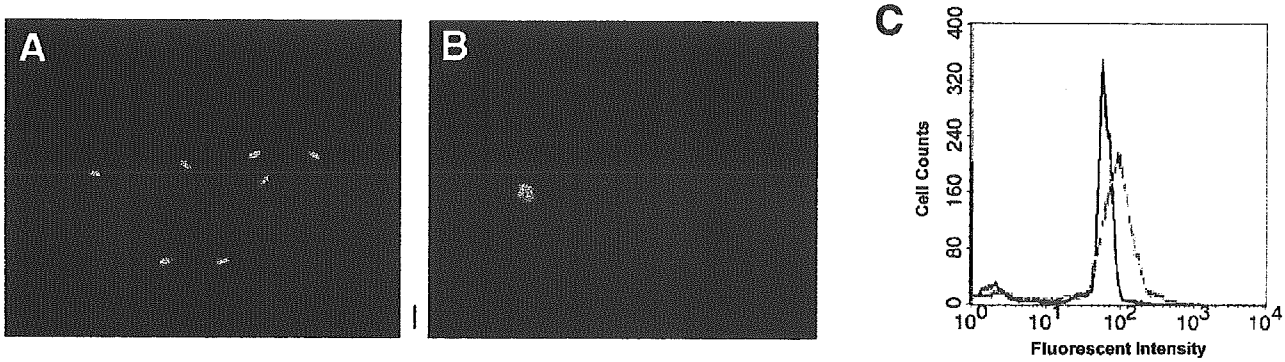

FIG. 8. Analysis of sperm from *Hanp1/H1T2* mutant mice. Sperm from heterozygous (A) and homozygous (B) *Hanp1/H1T2* mutant mice were stained with acridine orange (AO) and observed under UV light after being incubated in a medium containing 0.5 M β-mercaptoethanol. The nuclei of all sperm from homozygous mutant mice were disrupted by exposure to reducing conditions. Bar = 10 μm. (C) FACS analysis of sperm stained with propidium iodide (PI). Red and black indicate homozygous and heterozygous *Hanp1/H1T2* mutant sperm, respectively. Sperm from homozygous mice were stained more strongly and less homogeneously with PI than were control sperm.

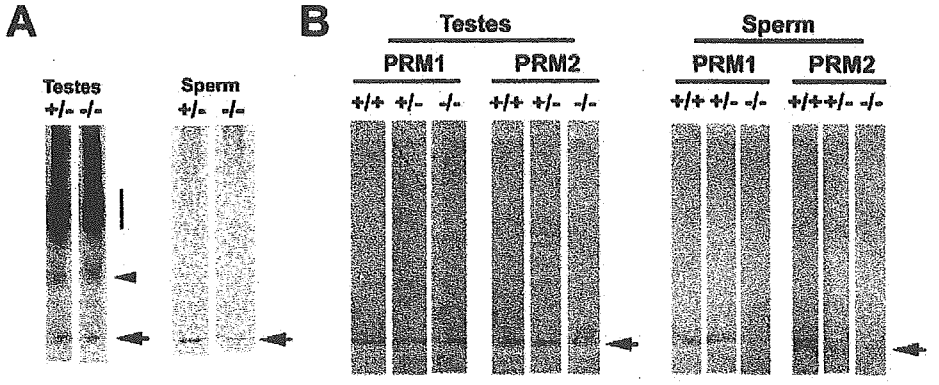

FIG. 9. Expression of protamine-1 and -2 in testes and sperm of *Hanp1/H1T2* mutant mice. Tissue lysates were electrophoresed in an acid-urea gel, and the proteins were stained with Coomassie brilliant blue (A) or subjected to Western blot analysis using anti-protamine monoclonal antibodies (B). Similar amounts of both protamine-1 and -2 (PRM1 and PRM2) were expressed in the testes of wild-type mice and of both homozygous and heterozygous *Hanp1/H1T2* mutant mice. In contrast, both protamines were only weakly detected in sperm from homozygous *Hanp1/H1T2* mutant mice (A). The arrows indicate the position of the protamine bands. The bar and arrowhead in panel A indicate the positions of histones and transition proteins, respectively.

observed after 1 h of incubation. The sperm from homozygous *Hanp1/H1T2* null mutant mice exhibited decreases in the ratio of motile sperm, the measurable velocities (including average path velocity, straight line velocity, and curvilinear velocity), and the amplitude of the lateral head displacement after 1 to 6 h of incubation compared with sperm from normal mice (data not shown). These observations indicated that the observed morphological abnormalities of the sperm from *Hanp1/H1T2* knockout mice may impair sperm movements and that the viability and maturation of the sperm are otherwise normal in these animals. The mutant sperm were insufficiently motile to fertilize eggs by in vitro fertilization (Table 2), although they could successfully bind to the zona pellucida in vitro. In contrast, *Hanp1/H1T2* mutant sperm could support fertilization and embryo development after ICSI. Sperm derived from two heterozygous and two homozygous *Hanp1/H1T2* mutant mice were injected into 92 and 106 eggs, respectively, from which 21 (27%) and 23 (28%) pups were born, respectively.

DNA is loosely packaged in *Hanp1/H1T2* null sperm. During normal chromatin remodeling in sperm, histones are replaced by protamines. Protamines form disulfide bond bridges, contributing to the chromatin in sperm nuclei being more densely packed than the chromatin in somatic cells. To examine the integrity of chromatin packaging in the homozygous *Hanp1/H1T2* mutant sperm, the reducing agent β-mercaptoethanol was added to sperm suspended in TYH medium. Although both wild-type and heterozygous *Hanp1/H1T2* mutant sperm tolerated the resulting reducing conditions without changes in nuclear morphology, all of the nuclei of the homozygous mutant sperm lost integrity (Fig. 8A and B). The chromatin packaging in the mutant sperm was also examined by staining the nuclear DNA with the intercalating dye propidium iodide and analyzing the cells by FACS (33). A substantial number of the sperm from homozygous *Hanp1/H1T2* mutants exhibited stronger staining and yielded a higher fluorescence peak than did the control sperm (Fig. 8C), indicating that propidium iodide had greater access to the nuclear DNA in the mutant sperm than in the wild-type sperm. Together, these observations suggested that the nuclei of sperm from *Hanp1/H1T2* mutant mice are easily disrupted and that the condensation of the nuclear DNA in *Hanp1/H1T2* mutant sperm is incomplete.

Protamine content is decreased in *Hanp1/H1T2* null sperm. Protamines are important molecules in the packaging of genomic DNA and the formation of the final chromatin pattern in sperm (5). Although normal levels of protamine-1 and -2 were detected in the testes of homozygous *Hanp1/H1T2* mutant mice, the levels detected in epididymal sperm were lower than those in controls (Fig. 9A). Western blotting with anti-protamine antibodies confirmed that the levels of both protamines in homozygous *Hanp1/H1T2* mutant sperm were quantitatively and/or qualitatively reduced (Fig. 9B) compared with the levels in sperm from wild-type mice. In contrast, there were no significant differences in the intensity of the protamine signal between the sperm from heterozygous and homozygous mice (Fig. 9A and 10). Furthermore, higher magnification images showed that both protamine-1 and -2 were highly restricted to the cell nuclei of elongated spermatids from heterozygous (Fig. 10) and wild-type mice (data not shown). In contrast, in elongated spermatids from homozygous *Hanp1/H1T2* mutant mice, protamine-1 was unevenly localized to the nuclei and aggregated around the nuclear region, and protamine-2 was distributed diffusely in the cytoplasm around the nuclei. Immunohistochemical observation of sperm with anti-protamine antibodies also showed minimal staining of the homozygous mutant sperm (Fig. 10B).

These results indicated that HANP1/H1T2 is necessary for the precise localization of protamines to the nuclei of elongated spermatids and spermatozoa and that the mutation of *Hanp1/H1T2* causes a substantial reduction in the protamine levels in the sperm or that protamines are not folded in the sperm nucleus in the same manner as in the wild-type but not in the testis.

DISCUSSION

Dramatic remodeling of chromatin takes place during mammalian spermiogenesis. Nuclear elongation and chromatin condensation occur concomitantly with modifications in the basic nuclear proteins associated with DNA. A number of

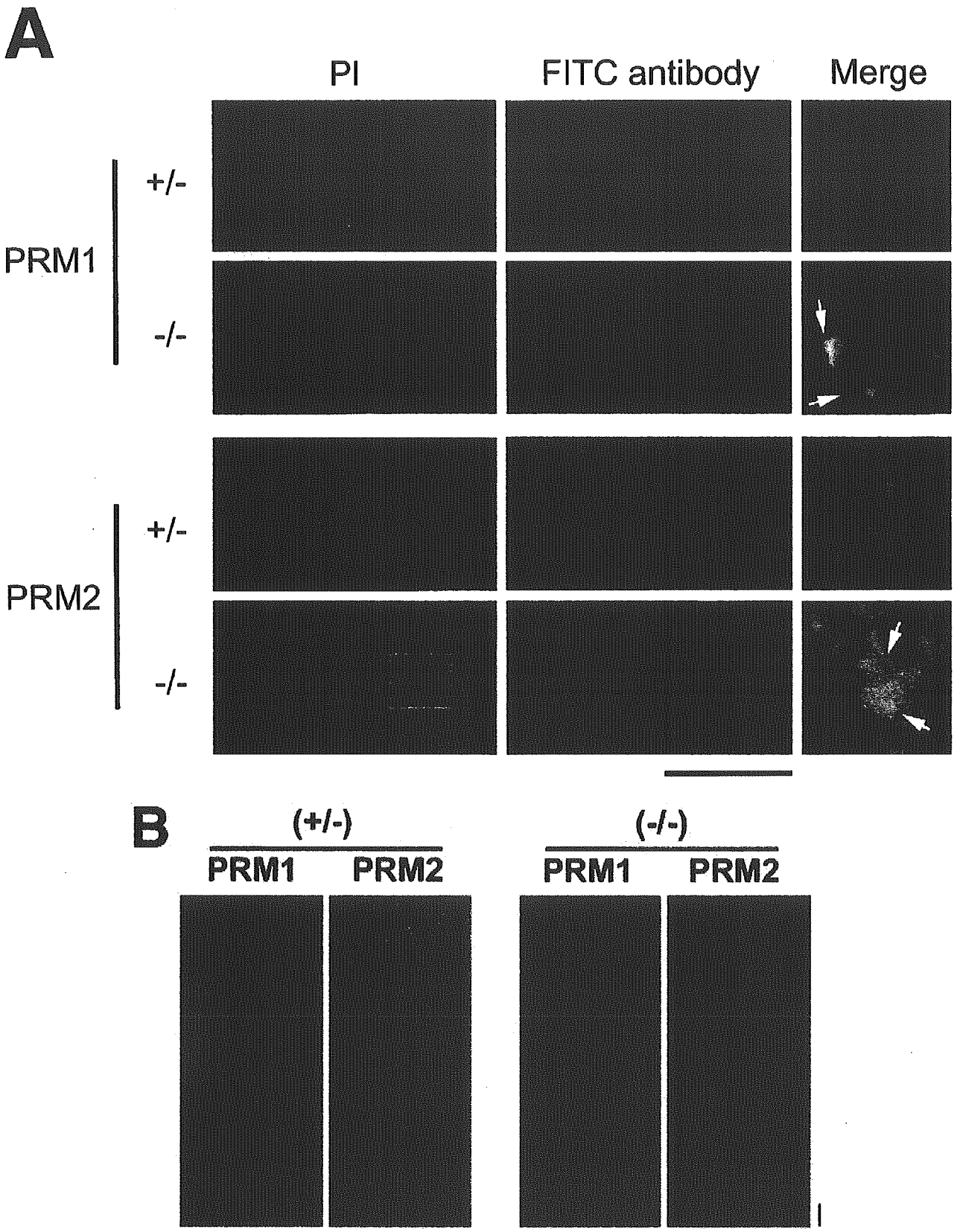
A
PI
FITC antibody
Merge
PRM1
+/-
-/-
PRM2
+/-
-/-
B
(+/-)
PRM1
PRM2
(-/-)
PRM1
PRM2

biochemical events accompany the displacement of histones and the appearance of a set of basic nuclear proteins such as tH2A, tH2B, H1t, spermatid-specific H2B (ssH2B), testis-specific HMG (tsHMG), histone H1-like protein in spermatids 1 (Hils 1), transition proteins (TNPs), and protamines (2, 3, 12, 13, 17, 20, 31). Histone synthesis ceases during spermiogenesis, and histones are replaced by a set of TNPs, which are subsequently replaced by protamines (2, 20). The completed process results in greater condensation of mitotic chromosomes, producing a tightly packaged chromatin structure. Recently, it was reported that some testicular nuclear proteins, such as protamines in sperm, have probably evolved from a primordial histone H1 (18). The chromatin structure of haploid germ cells has been complicated by the evolutionary replication of linker histone H1. Strong expression of linker histone H1 variants is important for the formation of sperm nuclei (21).

In this study, we identified a novel histone H1-like haploid germ-cell-specific nuclear protein designated HANP1/H1T2 that has an RS domain. HANP1/H1T2 is specifically expressed during chromatin remodeling and is mainly localized to the nucleus during spermiogenesis. Although homology of the complete amino acid sequence of HANP1/H1T2 with the histone H1 sequences of other organisms is not high (1), the homology with the globular H1 domain is substantial (35%). The HANP1/H1T2 protein in the mouse and its human homolog may also be evolutionarily derived from histone H1.

The finding that a portion of the endogenous HANP1/H1T2 in nuclear lysates of testicular germ cells was able to bind to DNA and that a substantial amount of HANP1/H1T2 was nonetheless recovered in the flowthrough fraction from DNA-cellulose columns indicated that HANP1/H1T2 protein, or its complexes, has two different forms with different DNA-binding abilities. HANP1/H1T2 protein also has an ATP-binding domain (23) and binds to ATP-cellulose columns. It has been reported that the functions of histones and other nuclear proteins are regulated by ATP and by phosphorylation (4, 8). Our findings therefore suggest that the DNA-binding ability of HANP1/H1T2 may be regulated by the binding of ATP to the ATP-binding domain. We attempted to examine the biochemistry of HANP1/H1T2 in more detail by purifying recombinant HANP1/H1T2 from *Escherichia coli* transformed with an expression vector. However, the transformed *E. coli* cells died rapidly, although expression of the recombinant protein was not induced. This observation suggests that a low level of "leaky" HANP1/H1T2 expression in *E. coli* was sufficient to induce cell death.

To investigate the physiological role of HANP1/H1T2 in chromatin condensation during spermiogenesis, we generated *Hanp1/H1T2* null mutant mice. The homozygous *Hanp1/H1T2* knockout mice exhibited aberrant chromatin packaging in the sperm nucleus and abnormal nuclear formation (14). Recent studies have suggested that the docking of protamine-1 to the nuclear envelope is an important intermediate step in spermiogenesis and have revealed novel roles for SR protein kinases and p32 (22). The observations that HANP1/H1T2 and protamines are expressed during similar steps of spermatid differentiation and that these proteins can be coimmunoprecipitated suggest that the recruitment of protamines into chromatin may be regulated by HANP1/H1T2, which has an RS domain. The HANP1/H1T2 protein colocalized with protamines in spermatid nuclei and associated with protamines in a direct or indirect manner, as supported by coimmunoprecipitation experiments using cotransfected HEK 293 cells in which no other spermatid-specific proteins were present. The observed abnormalities in the formation of spermatid nuclei in *Hanp1/H1T2* knockout mice indicated that HANP1/H1T2 might also be involved in chromatin formation during spermiogenesis.

Recent studies have shown that the inactivation of even one genome copy of either the protamine-1 or -2 gene resulted in the production of abnormal sperm and caused male infertility attributable to haploinsufficiency (5). Protamine-2 gene-deficient sperm, produced in chimeric mice resulting from injection of protamine-2 gene-deficient ES cells into wild-type blastocysts, were unable to induce embryonic development even by ICSI (6). Thus, the inability of sperm with reduced amounts of protamine-2 to successfully fertilize eggs or to induce embryogenesis is probably attributable to the loss of proper packaging of chromosomal DNA in the sperm, which, in turn, leaves the DNA susceptible to both damage and strand repair failure (6). In contrast, when homozygous *Hanp1/H1T2* mutant sperm were subjected to ICSI in this study, we obtained fairly efficient fertilization, normal embryogenesis, and healthy pups. Thus, it appears that the loss of protamines from sperm does not necessarily result in the deterioration of normal functioning of the sperm nuclei during fertilization, although sufficient protamine levels are important for proper chromatin and nuclear formation in spermatozoa. Alternatively, protamines may be important in spermiogenesis but not in the formation of the sperm head, such that a trace of protamine in the *Hanp1/H1T2* knockout sperm would be sufficient to support fertilization and development of embryos by ICSI, even though the packaging of the chromatin in the sperm was abnormal.

TNP1 and TNP2 are found in rodent spermatids, are be-

FIG. 10. Immunostaining of protamine-1 and -2 in the testes of heterozygous and homozygous *Hanp1/H1T2* mutant mice. PRM1 and PRM2 indicate immunofluorescent staining using anti-protamine-1 and -2 monoclonal antibodies, respectively. (A) Sections of testes. PI indicates nuclei stained with propidium iodide. The fluorescence signals of the secondary fluorescein isothiocyanate (FITC)-labeled anti-mouse antibody indicate that the localization of protamine-1 or -2 was limited to haploid spermatids during the later stages of differentiation (elongated spermatids). The area indicated by the white boxes was enlarged and merged. The signals of both protamine-1 and -2 were distributed in the nuclei of the control heterozygous mutant, whereas no nuclear-specific staining was observed in the homozygous *Hanp1/H1T2* mutant mice. The staining patterns of protamine-1 and -2 differed in the mutants (white arrows); the former appeared as dot-like aggregates in and around the nuclei, and the latter appeared as a diffuse staining in the cytoplasm around the nuclei. Bar = 50 μm. (B) Positively stained signals of both protamines were barely detectable in *hanp1* homozygous mutant sperm. Bar = 10 μm.

lieved to be the predominant transition proteins for chromatin remodeling in mammalian spermiogenesis, and are thought to be involved in histone displacement and chromatin condensation. Male mice with null mutations in either TNP1 or TNP2 were fertile, although their fertility was reported to be reduced (32, 33). However, mice in which both TNP genes were disrupted were completely sterile (34). The sperm produced by mice lacking both TNP1 and TNP2 contained immature protamines in the nuclei; the nuclei remained immature, the chromatin was incompletely packed by protamines, and the sperm nuclei were rapidly disrupted by exposure to reducing conditions (34). Although the double-mutant nuclei could successfully support embryogenesis after ooplasmic round spermatid-nuclear injection, no pups were produced by ICSI (34). This differs from our ICSI results using sperm from homozygous *Hanp1/H1T2* knockout mice. Together, these results indicate that the nuclei of sperm from mice with both TNPs disrupted are more unstable than those of sperm from homozygous *Hanp1/H1T2* knockout mice. The abnormal distribution of protamine-1 and -2 in some elongated spermatids in the testes of homozygous *Hanp1/H1T2* knockout mice suggests that HANP1/H1T2 is involved in chromatin remodeling, together with TNPs. Thus, to further the understanding of the role of HANP1/H1T2 in chromatin remodeling, it will be necessary to investigate the associations between HANP1/H1T2 and other nuclear proteins, as well as those between TNPs and protamines.

Our results indicate that HANP1/H1T2 is a novel protein essential for the packaging of protamine and DNA into chromatin in sperm and for the formation of the compact sperm nucleus that is required for natural fertilization. However, these conditions are not necessarily prerequisites for the production of healthy pups if the initial process of fertilization is bypassed by assisted microfertilization. We suggest that mutations or disruptions of the *Hanp1/H1T2* gene may underlie some cases of human infertility. In addition, future research on the biochemical characteristics of HANP1/H1T2 may contribute to an understanding of the formation of the nucleus during spermiogenesis.

ACKNOWLEDGMENTS

We acknowledge IngenKO Pty. Ltd., Australia, for their help in producing the *Hanp1/H1T2* mutant mice. We thank Balhorn Rod for providing the monoclonal antibodies to protamine-1 and -2. We also thank Hiromi Nishimura, Kahori Numazawa, and Amy Herlihy for their technical assistance, and Textcheck and Stephanie L. Cook for editing the manuscript.

REFERENCES

1. **Ali, T., P. Coles, T. J. Stevens, K. Stott, and J. O. Thomas.** 2004. Two homologous domains of similar structure but different stability in the yeast linker histone, Hho1p. J. Mol. Biol. **338**:139–148.
2. **Balhorn, R.** 1982. A model for the structure of chromatin in mammalian sperm. J. Cell Biol. **93**:298–305.
3. **Boissonneault, G., and Y. F. Lau.** 1993. A testis-specific gene encoding a nuclear high-mobility-group box protein located in elongating spermatids. Mol. Cell. Biol. **13**:4323–4330.
4. **Cheung, P., C. D. Allis, and P. Sassone-Corsi.** 2000. Signaling to chromatin through histone modifications. Cell **103**:263–271.
5. **Cho, C., W. D. Willis, E. H. Goulding, H. Jung-Ha, Y. C. Choi, N. B. Hecht, and E. M. Eddy.** 2001. Haploinsufficiency of protamine-1 or -2 causes infertility in mice. Nat. Genet. **28**:82–86.
6. **Cho, C., H. Jung-Ha, W. D. Willis, E. H. Goulding, P. Stein, Z. Xu, R. M. Schultz, N. B. Hecht, and E. M. Eddy.** 2003. Protamine 2 deficiency leads to sperm DNA damage and embryo death in mice. Biol. Reprod. **69**:211–217.
7. **de Rooij, D. G., M. Okabe, and Y. Nishimune.** 1999. Arrest of spermatogonial differentiation in jsd/jsd, Sl17H/Sl17H, and cryptorchid mice. Biol. Reprod. **61**:842–847.
8. **Dou, Y., and M. A. Gorovsky.** 2000. Phosphorylation of linker histone H1 regulates gene expression *in vivo* by creating a charge patch. Mol. Cell **6**:225–231.
9. **Fujii, T., K. Tamura, K. Masai, H. Tanaka, Y. Nishimune, and H. Nojima.** 2002. Use of stepwise subtraction to comprehensively isolate mouse genes whose transcription is up-regulated during spermiogenesis. EMBO Rep. **3**:367–372.
10. **Graveley, B. R.** 2004. A protein interaction domain contacts RNA in the prespliceosome. Mol. Cell **13**:302–304.
11. **Ho, Y., K. Wigglesworth, J. J. Eppig, and R. M. Schultz.** 1995. Preimplantation development of mouse embryos in KSOM: augmentation by amino acids and analysis of gene. Mol. Reprod. Dev. **41**:232–238.
12. **Huh, N. E., I. W. Hwang, K. Lim, K. H. You, and C. B. Chae.** 1991. Presence of a bi-directional S phase-specific transcription regulatory element in the promoter shared by testis-specific TH2A and TH2B histone genes. Nucleic Acids Res. **19**:93–98.
13. **Iguchi, N., H. Tanaka, K. Yomogida, and Y. Nishimune.** 2003. Isolation and characterization of a novel cDNA encoding a DNA-binding protein (Hils1) specifically expressed in testicular haploid germ cells. Int. J. Androl. **26**:354–365.
14. **Kimura, T., C. Ito, S. Watanabe, T. Takahashi, M. Ikawa, K. Yomogida, Y. Fujita, M. Ikeuchi, N. Asada, K. Matsumiya, A. Okuyama, M. Okabe, K. Toshimori, and T. Nakano.** 2003. Mouse germ cell-less as an essential component for nuclear integrity. Mol. Cell. Biol. **23**:1304–1315.
15. **Kimura, Y., and R. Yanagimachi.** 1995. Intracytoplasmic sperm injection in the mouse. Biol. Reprod. **52**:709–720.
16. **Koga, M., H. Tanaka, K. Yomogida, M. Nozaki, J. Tsuchida, H. Ohta, Y. Nakamura, K. Masai, Y. Yoshimura, M. Yamanaka, N. Iguchi, H. Nojima, K. Matsumiya, A. Okuyama, and Y. Nishimune.** 2000. Isolation and characterization of a haploid germ cell-specific novel complementary deoxyribonucleic acid; testis-specific homologue of succinyl CoA:3-Oxo acid CoA transferase. Biol. Reprod. **63**:1601–1609.
17. **Kremer, E. J., and W. S. Kistler.** 1991. Localization of mRNA for testis-specific histone H1t by *in situ* hybridization. Exp. Cell Res. **197**:330–332.
18. **Lewis, J. D., N. Saperas, Y. Song, M. J. Zamora, M. Chiva, and J. Ausio.** 2004. Histone H1 and the origin of protamines. Proc. Natl. Acad. Sci. USA **101**:4148–4152.
19. **Li, E.** 2002. Chromatin modification and epigenetic reprogramming in mammalian development. Nat. Rev. Genet. **3**:662–673.
20. **Mali, P., A. Kaipia, K. Kangasniemi, J. Toppari, M. Sandberg, N. B. Hecht, and M. Parvinen.** 1989. Stage-specific expression of nucleoprotein mRNAs during rat and mouse spermiogenesis. Reprod. Fertil. Dev. **1**:369–382.
21. **Martianov, I., S. Brancorsini, R. Catena, A. Gansmuller, N. Kotaja, M. Parvinen, P. Sassone-Corsi, and I. Davidson.** 2005. Polar nuclear localization of H1T2, a histone H1 variant, required for spermatid elongation and DNA condensation during spermiogenesis. Proc. Natl. Acad. Sci. USA **102**: 2808–2813.
22. **Mylonis, I., V. Drosou, S. Brancorsini, E. Nikolakaki, P. Sassone-Corsi, and T. Giannakouros.** 2004. Temporal association of protamine 1 with the inner nuclear membrane protein lamin B receptor during spermiogenesis. J. Biol. Chem. **279**:11626–11631.
23. **Neuwald, A. F., L. Aravind, J. L. Spouge, and F. Koonin.** 1999. AAA+: a class of chaperone-like ATPases associated with the assembly, operation, and disassembly of protein complexes. Genome Res. **9**:27–43.
24. **Russell, L. D., R. A. Ettlin, H. A. P. Sinha, and E. D. Clegg.** 1990. Mammalian spermatogenesis, p. 1–40. *In* L. D. Russell, R. A. Ettlin, H. A. P. Sinha, and E. D. Clegg (ed.), Histological and histopathological evaluation of the testis. Cache River Press, St. Louis, Mo.
25. **Sassone-Corsi, P.** 2002. Unique chromatin remodeling and transcriptional regulation in spermatogenesis. Science **296**:2176–2178.
26. **Stanker, L. H., A. Wyrobek, and R. Balhorn.** 1987. Monoclonal antibodies to human protamines. Hybridoma **6**:293–303.
27. **Tanaka, H., L. A. Pereira, M. Nozaki, J. Tsuchida, K. Sawada, H. Mori, and Y. Nishimune.** 1997. A germ cell-specific nuclear antigen recognized by a monoclonal antibody raised against mouse testicular germ cells. Int. J. Androl. **20**:361–366.
28. **Tanaka, H., N. Iguchi, Y. Toyama, K. Kitamura, T. Takahashi, K. Kaseda, M. Maekawa, and Y. Nishimune.** 2004. Mice deficient for the axonemal protein tektin-t exhibit male infertility and immotile cilia syndrome due to impaired inner arm dynein function. Mol. Cell. Biol. **24**:7956–7964.
29. **Tanaka, H., and T. Baba.** 2005. Gene expression in spermiogenesis. Cell. Mol. Life Sci. **62**:344–354.
30. **Toyoda, Y., M. Yokoyama, and T. Hoshi.** 1971. Studies on the fertilization of mouse egg *in vitro*. Jpn. J. Anim. Reprod. **16**:147–151.
31. **Yan, W., L. Ma, K. H. Burns, and M. M. Matzuk.** 2003. HILS1 is a sper-

matid-specific linker histone H1-like protein implicated in chromatin remodeling during mammalian spermiogenesis. Proc. Natl. Acad. Sci. USA **100:** 10546–10551.

32. **Yu, Y. E., Y. Zhang, E. Unni, C. R. Shirley, J. M. Deng, L. D. Russell, M. M. Weil, R. R. Behringer, and M. L. Meistrich.** 2000. Abnormal spermatogenesis and reduced fertility in transition nuclear protein 1-deficient mice. Proc. Natl. Acad. Sci. USA **97:**4683–4688.
33. **Zhao, M., C. R. Shirley, Y. E. Yu, B. Mohapatra, Y. Zhang, E. Unni, J. M. Deng, N. A. Arango, N. H. Terry, M. M. Weil, L. D. Russell, R. R. Behringer, and M. L. Meistrich.** 2001. Targeted disruption of the transition protein 2 gene affects sperm chromatin structure and reduces fertility in mice. Mol. Cell. Biol. **21:**7243–7255.
34. **Zhao, M., C. R. Shirley, S. Hayashi, L. Marcon, B. Mohapatra, R. Suganuma, R. R. Behringer, G. Boissonneault, R. Yanagimachi, and M. L. Meistrich.** 2004. Transition nuclear proteins are required for normal chromatin condensation and functional sperm development. Genesis **38:**200–213.

Dysregulation of TGF-β1 receptor activation leads to abnormal lung development and emphysema-like phenotype in core fucose-deficient mice

Xiangchun Wang[a,b], Shinya Inoue[a,b,c], Jianguo Gu[a], Eiji Miyoshi[a], Katsuhisa Noda[a], Wenzhe Li[d], Yoko Mizuno-Horikawa[a], Miyako Nakano[a], Michio Asahi[a], Motoko Takahashi[a,e], Naofumi Uozumi[a], Shinji Ihara[a], Seung Ho Lee[a], Yoshitaka Ikeda[a,e], Yukihiro Yamaguchi[a,f], Yoshiya Aze[g], Yoshiaki Tomiyama[c], Junichi Fujii[a,h], Keiichiro Suzuki[a,f], Akihiro Kondo[d], Steven D. Shapiro[i], Carlos Lopez-Otin[j], Tomoyuki Kuwaki[k], Masaru Okabe[l], Koichi Honke[a,m], and Naoyuki Taniguchi[a,n]

Departments of [a]Biochemistry, [c]Internal Medicine and Molecular Science, and [d]Glycotherapeutics, Osaka University Graduate School of Medicine, Osaka 565-0871, Japan; [e]Department of Cell Biology, Saga University School of Medicine, Saga 809-8501, Japan; [f]Department of Biochemistry, Hyogo College of Medicine, Hyogo 663-8501, Japan; [g]Fukui Safety Institute, Ono Pharmaceutical Co., Fukui 913-8538, Japan; [h]Department of Biochemistry, Yamagata University School of Medicine, Yamagata 990-9585, Japan; [i]Department of Medicine, Section of Pulmonary and Critical Care Medicine, Brigham and Women's Hospital, Boston, MA 02115; [j]Departamento de Bioquimica y Biologia Molecular, Instituto Universitario de Oncologia, Universidad de Oviedo, 33006 Oviedo, Spain; [k]Department of Molecular and Integrative Physiology, Graduate School of Medicine, Chiba University, Chiba 260-8670, Japan; [l]Department of Experimental Genome Research, Genome Information Research Center, Osaka University, Osaka 565-0871, Japan; and [m]Department of Molecular Genetics, Kochi University Medical School, Kochi 783-8505, Japan

Communicated by David H. MacLennan, University of Toronto, Toronto, ON, Canada, August 24, 2005 (received for review August 2, 2005)

The core fucosylation (α1,6-fucosylation) of glycoproteins is widely distributed in mammalian tissues, and is altered under pathological conditions. To investigate physiological functions of the core fucose, we generated α1,6-fucosyltransferase (*Fut8*)-null mice and found that disruption of *Fut8* induces severe growth retardation and death during postnatal development. Histopathological analysis revealed that *Fut8*$^{-/-}$ mice showed emphysema-like changes in the lung, verified by a physiological compliance analysis. Biochemical studies indicated that lungs from *Fut8*$^{-/-}$ mice exhibit a marked overexpression of matrix metalloproteinases (MMPs), such as MMP-12 and MMP-13, highly associated with lung-destructive phenotypes, and a down-regulation of extracellular matrix (ECM) proteins such as elastin, as well as retarded alveolar epithelia cell differentiation. These changes should be consistent with a deficiency in TGF-β1 signaling, a pleiotropic factor that controls ECM homeostasis by down-regulating MMP expression and inducing ECM protein components. In fact, *Fut8*$^{-/-}$ mice have a marked dysregulation of TGF-β1 receptor activation and signaling, as assessed by TGF-β1 binding assays and Smad2 phosphorylation analysis. We also show that these TGF-β1 receptor defects found in *Fut8*$^{-/-}$ cells can be rescued by reintroducing *Fut8* into *Fut8*$^{-/-}$ cells. Furthermore, exogenous TGF-β1 potentially rescued emphysema-like phenotype and concomitantly reduced MMP expression in *Fut8*$^{-/-}$ lung. We propose that the lack of core fucosylation of TGF-β1 receptors is crucial for a developmental and progressive/destructive emphysema, suggesting that perturbation of this function could underlie certain cases of human emphysema.

fucosylation | glycobiology | matrix metalloproteinase

The physiological importance of fucose modifications on proteins has been highlighted recently by the description of human congenital disorders of glycosylation (CDG). The disease CDG-IIc is due to lack of the GDP-fucose transporter activity (1, 2). α1,2-, α1,3-, α1,4-, and α1,6-fucosylations have been described; α1,6-fucose is found linked to the Asn-linked GlcNAc in the *N*-glycan core. All of these fucosylations are terminal capping reactions, and the fucose residues have no substituent. In contrast, O-fucosylation, in which fucose is attached directly to a serine or threonine residue in a particular protein context such as an EGF repeat, undergoes the elongation of the oligosaccharide into a tetrasaccharide (NeuAcα2–3/6Galβ1–4GlcNAcβ1–3Fuc-Ser/Thr), in which Fringe has been found to be the *N*-acetylglucosaminyltransferase acting on O-linked fucose of the Notch receptor (3). Because Notch receptors play key roles in numerous developmental events, several features of the phenotype in CDG-IIc could be explained by defects in Notch function. However, Sturla *et al.* (4, 5) reported that reduced fucosylation is mainly confined to terminal fucosylation of *N*-glycans, and that protein O-fucosylation levels such as those that occur in Notch are unaffected in CDG-IIc; therefore, we speculate that core fucosylation may be responsible for the phenotype of CDG-IIc.

GDP-L-Fuc:*N*-acetyl-β-D-glucosaminide α1,6-fucosyltransferase (Fut8, EC 2.4.1.152) catalyzes the transfer of a fucose residue from GDP-fucose to position 6 of the innermost GlcNAc residue of hybrid and complex types of N-linked oligosaccharides on glycoproteins (6). Core Fut8 is the only core FucT in mammals, but there are core α1,3-Fuc residues in plants, insects, and probably other species. The *Fut8* gene is expressed in most rat organs with a relatively high level of expression in brain and small intestine (7). In good agreement with the *Fut8* gene expression, α1,6-fucosylated glycoproteins are widely distributed in mammalian tissues (8). Furthermore, the expression of Fut8 and the extent of core fucosylation are altered under pathological conditions such as hepatocellular carcinoma and liver cirrhosis (8, 9).

The molecular cloning of the *Fut8* gene (10) enabled us to manipulate it and to remodel the *N*-glycans in animal models. Overexpression of the *Fut8* gene caused steatosis in the liver and kidney due to a decreased lysosomal acid lipase activity accompanied by its over-fucosylation (11). Recently, it was reported that the core fucose-deficient IgG1 (produced in a fucose-deficient Chinese hamster ovary cell line) showed improved binding to FcγRIIIA. As a consequence, antibody-dependent cellular cytotoxicity activity mediated by their interaction was enhanced (12, 13). These findings strongly suggested that core fucosylation of *N*-glycans modifies the function of the glycoproteins.

To define the physiological roles of a particular glycosylation, gene targeting technology to disrupt the relevant glycosyltrans-

Freely available online through the PNAS open access option.

Abbreviations: ECM, extracellular matrix; MMP, matrix metalloproteinase; PA, 2-aminopyridine.

See Commentary on page 15721.

[b]X.W. and S. Inoue contributed equally to this work.

[n]To whom correspondence should be addressed at: Department of Biochemistry, Osaka University Graduate School of Medicine, 2-2 Yamadaoka, Suita, Osaka 565-0871, Japan. E-mail: proftani@biochem.med.osaka-u.ac.jp.

ferase gene function is considered as the best approach currently available. In fact, accumulating evidence on gene targeting for glycosyltransferases has elucidated a variety of novel functions of carbohydrates and provided new insights into their roles *in vivo* (14). Here we report the generation of *Fut8*-null mice and describe critical roles of core fucosylation *in vivo*.

Materials and Methods

Gene Targeting. A part of the mouse *Fut8* gene spanning 13.9 kb, which includes the exon containing the translation-initiation site, was isolated by screening a mouse 129SvJ λ genomic library (Stratagene), using a SacI–SacI fragment of porcine *Fut8* cDNA (nt −39 to 373) (10) as a probe. A targeting vector was constructed by replacing the 184-bp SacI–HindIII fragment containing the translation-initiation site with a 4.9-kb SacI–SalI fragment of the plasmid pGT1.8IresBgeo (15) that contains an internal ribosome entry site (*IRES*)-*LacZ-Neo*'- polyadenylation signal (*pA*) cassette, flanked with a 1.5-kb XhoI–NotI fragment of the plasmid pMC1DTpA (16), which encodes diphtheria toxin A chain (*DT-A*) for negative screening (see Fig. 4, which is published as supporting information on the PNAS web site). The targeting vector was transfected into D3 embryonic stem cells, and clones were selected with G418. Southern blot analysis of selected clones with 5′ (*A*) and 3′ (*B*) probes (Fig. 4) revealed that 1.2% (4 of 343) of the embryonic stem clones had undergone correct homologous recombination. Targeted cell clones were then injected into blastocysts from B6C3F1 mice, which are F_1 mice resulting from the intercross of female C57BL/6 and male C3H mice. Germ-line transmission of the mutant allele was achieved from male chimeras derived from two independent embryonic stem cell clones.

Oligosaccharide Structural Analyses of the Mouse Lungs. N-linked oligosaccharides of lung were liberated by hydrazinolysis at 100°C for 10 h and then re-N-acetylated. The reducing ends of the oligosaccharides were labeled with 2-aminopyridine (PA) as described in ref. 17. PA-oligosaccharides were subjected to HPLC analysis and further to liquid chromatography–electrospray ionization–MS analysis, which was performed on an HCT ion trap mass spectrometer (Bruker Daltonics, Bremen, Germany) equipped with an electrospray source working in positive ion mode.

Measurement of Lung Compliance and Ventilation. Lung compliance was measured by drawing static air pressure–volume relations in urethane-anesthetized (1.5 g/kg) mice tracheotomized with polyethylene tubing (O.D. = 0.8 mm). Total lung capacity was defined as the lung volume of full inflation as judged by visual inspection of the lung that fully occupied the chest cavity. Any obvious, continual decrease in the pressure was evidence of a leaking lung, which was then discarded. The lung volumes at each measured point were expressed as a percentage of the total lung capacity. Ventilation was measured by whole-body plethysmography in unanesthetized freely moving mice as reported in ref. 18.

Establishment of Embryonic Fibroblasts. For preparation of embryonic fibroblasts, a whole mouse embryo at 18.5 days postcoitus was dissected, and the head and all internal organs were removed. The carcasses were minced, incubated in PBS (−) containing 0.05% trypsin, 0.53 mM EDTA, and 40 μg/ml DNase at 37°C for 30 min with stirring three times, and then cells were plated on a 100-mm dish in DMEM supplemented with 10% FCS and incubated at 37°C in humidified air containing 5% CO_2. To obtain immortal cells, Zeocine-resistant vector (pcDNA3.1) containing the SV40 gene was introduced to these primary embryonic fibroblasts. Transfectants were screened in the presence of 400 μg/ml Zeocine, and SW (wild-type cells immortalized with SV40 gene) and SK (knockout cells immortalized with SV40 gene) immortal cells were established from $Fut8^{+/+}$ and $Fut8^{-/-}$ primary fibroblasts, respectively.

^{125}I-TGF-β1-Binding Assays. The cells (1.5×10^5 per well) were cultured on 24-well plates, washed twice with 500 μl of PBS containing 0.1% BSA, and incubated with 200 μl of PBS containing different amounts of ^{125}I-TGF-β1 in a concentration range of 0.1–1.0 ng and 10 ng of unlabeled TGF-β1. Nonspecific binding was determined by adding 100 ng of unlabeled TGF-β1. After incubation for 2 h at 4°C with shaking, the cells were washed and solubilized in 500 μl of 1 M NaOH. The radioactivity of the cell lysates was counted with a γ-counter.

Receptor Cross-Linking. The cells (5×10^5) were seeded onto a 60-mm culture dish and incubated for 48 h. After being washed with cool PBS containing 0.1% BSA, the cells were incubated for 2 h at 4°C with 250 pM ^{125}I-TGF-β1 and then incubated with 1 mM cross-linking reagent BS^3 for 30 min at room temperature. After washing, the cells were lysed, the protein concentrations of cell lysates were determined, and the same amounts of protein were loaded onto 10% SDS-polyacrylamide gel for analysis. The gels were exposed and quantified with the BAS-2500 bio-imaging analyzer (Fuji).

Immunohistochemical Analysis. To detect the P-Smad2 (Ser-465/467), matrix metalloproteinase (MMP)-12, or SP-C, whole lung tissues from animals after age indicated were fixed in 0.1 M PBS containing 4% paraformaldehyde and embedded in paraffin. For immunohistochemical analysis, the dewaxed sections were pretreated with avidin-biotin blocking and hydroxygen blocking for 10 min at 37°C, and then incubated with rabbit anti-P-Smad2 antibody (Cell Signaling Technology, Beverly, MA), anti-MMP-12 antibody, or anti-SP-C antibody (Santa Cruz Biotechnology) for 16 h at 4°C. Localization of the first antibody was visualized by an avidin-biotin coupling (ABC) immunoperoxidase technique, using a commercial kit (Vector Laboratories) according to the manufacturer's instructions.

Therapeutic Administration of Exogenous TGF-β1 to *Fut8*$^{-/-}$ Mice. We performed i.p. injection of recombinant TGF-β1 in a dose of 50 or 100 ng/g of mouse body weight to postnatal 18-day $Fut8^{-/-}$ mice. After 20 times of injection every 2 days, lung sections were subjected to hematoxylin/eosin staining or immunohistochemical study.

Results and Discussion

***Fut8* Gene Is a Unique Fucosyltransferase Responsible for the Core Fucosylation of *N*-Glycans.** A targeted disruption of *Fut8* was generated through homologous recombination in embryonic stem cells. The targeting vector was constructed by replacing exon 2 of *Fut8*, which contains the translation initiation site, with an IRES-LacZ-Neo-pA cassette (Fig. 4*A*). Genotypes of pups from intercrosses between heterozygous mice were determined by Southern blotting (Fig. 4*B*). The phenotype described here was identical in two lines. Northern blot analysis of lung and brain RNA revealed that expression of full-length *Fut8* mRNA was abolished in homozygous mutant mice, whereas *Fut8* transcripts were detected as a single 3.5-kb band in wild-type mice (Fig. 4*C*). Consistent with this finding, Fut8 activity could not be detected in $Fut8^{-/-}$ tissues including brain or lung, even with six times longer incubation than that used for $Fut8^{+/+}$ specimens (Fig. 4*D* and data not shown). Furthermore, the analysis of *N*-glycan structures showed that the elution profile of $Fut8^{-/-}$ lung lacked the peaks of oligosaccharides with core fucose eluting at 30–35 min, as described in refs. 19 and 20 (Fig. 4*E*). These oligosaccharides were also confirmed by mass spectrometric analysis (Fig. 5, which is published as supporting information on the PNAS web site). This finding agrees with previous reports indicating that there are no additional genes homologous to *Fut8* in mammals and lower organisms (21, 22). Thus, the *Fut8* gene is the only one responsible for the core fucosylation of *N*-glycans in mouse tissues.

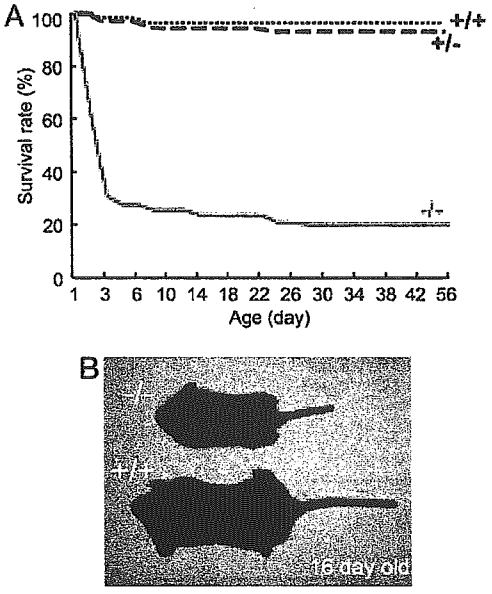

Fig. 1. Semilethality and growth retardation in *Fut8*$^{-/-}$ mice. (*A*) Survival ratio of *Fut8*$^{-/-}$ (−/−, solid line), *Fut8*$^{+/-}$ (+/−, broken line), and *Fut8*$^{+/+}$ (+/+, dotted line) mice after birth. (*B*) A 16-day-old *Fut8*$^{-/-}$ pup (−/−) with a *Fut8*$^{+/+}$ littermate (+/+).

Core Fucosylation Is Essential for Mice Survival and Growth. *Fut8*$^{-/-}$ mice were born apparently healthy with almost the expected Mendelian inheritance: Of 277 pups, there were 59 (21.3%) *Fut8*$^{-/-}$, 147 (53.1%) *Fut8*$^{+/-}$, and 71 (25.6%) *Fut8*$^{+/+}$ mice. At embryonic day 19, frequencies of *Fut8*$^{-/-}$, *Fut8*$^{+/-}$, and *Fut8*$^{+/+}$ mice were 26, 52, and 22 of 100 embryos, and there were no apparent anomalies in *Fut8*$^{-/-}$ mice. In contrast to *Fut8*$^{-/-}$ mice, embryonic lethality was observed in mutant mice deficient in the FX gene, which encodes an enzyme in the *de novo* pathway for GDP-fucose synthesis and is responsible for all cellular fucosylation, e.g., α1,2; α1,3; α1,6; etc. (23). The appearance of *Fut8*$^{-/-}$ mice could not be distinguished from *Fut8*$^{+/-}$ and *Fut8*$^{+/+}$ mice within 3 days of age, but $\approx$70% of them died during this period (Fig. 1*A*). Most of the survivors manifested severe growth retardation (Fig. 1*B*). This pattern observed in the *Fut8*$^{-/-}$ mice is quite different from other N-linked medial- and trans-Golgi glycosyltransferases, such as GnT-III-, GnT-V-, or ST6Gal1-null mice (14), suggesting that core fucose has a unique role in the regulation of proliferation and differentiation after birth.

Progressive Emphysema-Like Changes in *Fut8*$^{-/-}$ Lungs. Histological analyses by hematoxylin/eosin staining of 3-, 7-, 10-, and 18-day-old and 8-week-old *Fut8*$^{-/-}$ mice showed a symmetrical reduction in the size of most organs, which otherwise appeared devoid of pathological signs. The lungs of *Fut8*$^{-/-}$ mice, however, apparently displayed generalized air-space enlargement and dilated alveolar ducts, compared with those of *Fut8*$^{+/+}$ and *Fut8*$^{+/-}$ mice (Fig. 2*A*). The mean linear intercept was calculated at the ages indicated. From postnatal day 7, diameters of the pulmonary alveoli of *Fut8*$^{-/-}$ mice were increased significantly, compared with those in *Fut8*$^{+/+}$ mice (Fig. 2*B*). To evaluate the functional relevance of this morphological abnormality, lung compliance was evaluated by a static air deflation curve (Fig. 2*C*). The *Fut8*$^{-/-}$ lungs had larger total lung capacities and increased lung compliance compared with *Fut8*$^{+/-}$ and *Fut8*$^{+/+}$ lungs. These results indicate that the altered architecture of the enlarged *Fut8*$^{-/-}$ mouse airspace contributes to the increased compliance. We also measured pressure–volume relationships in body-weight-matched young wild types ($\approx$7 days old) to cancel the difference in total lung capacity. Again, static lung compliance in *Fut8*$^{-/-}$ mice was greater than that in wild-type mice (data not shown). When *Fut8*$^{-/-}$ mice breathed room air under resting conditions, respiratory minute volume and rate, as determined by body plethysmography, were higher than in wild-type mice. Ventilatory responses to systemic hypoxia (12% O_2) or hypercapnia (5% CO_2/21% O_2), or increases in the respiratory minute volume, were significantly attenuated in *Fut8*$^{-/-}$ mice, compared with *Fut8*$^{+/+}$ and *Fut8*$^{+/-}$ mice (Fig. 2*D*). These findings, although not specific markers of emphysema, suggest that *Fut8* is involved in the physiological control of ventilation. However, we do not believe that the main reason that *Fut8*$^{-/-}$ mice die is lung disorder. Interestingly, besides TGF-β1 receptor as described below, we also found that loss of core fucosylation resulted in modest down-regulation of several other receptors-mediated signaling, such as EGF receptor and integrins (unpublished data), which are responsible for cell growth and differentiation. Therefore, we would like to take the hypothesis that the growth retardation and early death of *Fut8*$^{-/-}$ mice can be attributed to dysregulation of many receptors-mediated signaling.

Enhanced Expression Levels of MMPs in *Fut8*$^{-/-}$ Lungs and *Fut8*$^{-/-}$ Cells. Pulmonary emphysema is believed to result from decreased structural integrity of connective tissues due to a defect in their formation or to an abnormal proteolysis. Elastin and fibrillar collagen are major components of the extracellular matrix (ECM), which sustains the normal lung architecture. On the other hand, MMPs are a group of zinc- and calcium-dependent proteinases that have an important role in the normal turnover of ECM components. Abnormal production of MMPs is implicated in the induction of emphysema. Thus, transgenic mice expressing human MMP-1 develop emphysema through destruction of collagen fibrils (24). Furthermore, MMP-2, MMP-9, and MMP-12 lead to emphysema by degradation of elastin fibers (25, 26). Therefore, expression levels of collagens, elastin, and a number of MMPs of putative relevance in lung pathology, including McolB (a mouse orthologue of human MMP-1) (27) and MMP-2, -8, -9, -12, -13, and -14, were examined in the lungs of Fut8-mutant mice. RT-PCR analysis showed that there were no significant changes in the expression levels of collagens, MMP-2, -8, and -14 in lung tissues from *Fut8*$^{-/-}$, *Fut8*$^{+/-}$, and *Fut8*$^{+/+}$ mice (Fig. 3*A*). However, expression levels of McolB, MMP-12, and MMP-13 were greatly enhanced (Fig. 3*A*); in addition, a slight increase in MMP-9 levels was detected in lungs from *Fut8*$^{-/-}$ by using real-time RT-PCR (Fig. 6*A* and Table 2, which are published as supporting information on the PNAS web site). Conversely, elastin expression was down-regulated in lungs from Fut8-deficient mice. On the other hand, fragmentation and a significantly reduced number of elastic fibers were observed by elastin staining in *Fut8*$^{-/-}$ mice (Fig. 6*B*), supporting the view that the degrading phenotype, i.e., emphysematous changes, occurs in *Fut8*$^{-/-}$ lung. Actually, emphysema-like changes were coincident with increased expression levels of MMP-12 from postnatal day 7 of *Fut8*$^{-/-}$ mice (Fig. 6*C*). Furthermore, only in the bronchoalveolar lavage fluid of *Fut8*$^{-/-}$ mice did macrophages look vacuolated, which, along with MMP-12 expression, indicates activation (Fig. 6*I*). In addition, an enhanced expression of CD68, a marker of macrophage, was clearly observed in *Fut8*$^{-/-}$ lung (data not shown). Recently, Morris *et al.* (28) reported that the loss of the epithelial integrin αVβ6, which causes a local deficiency in active TGF-β1, results in the increased expression of MMP-12 and leads to a slowly progressive, age-related emphysema. Likewise, McolB is a murine orthologue of human MMP-1, an enzyme that has been associated repeatedly with lung pathology, including emphysema (24), whereas MMP-13 or collagenase-3 is a very potent enzyme with wide substrate specificity, which is also associated with pulmonary diseases. It will also be interesting to examine whether core

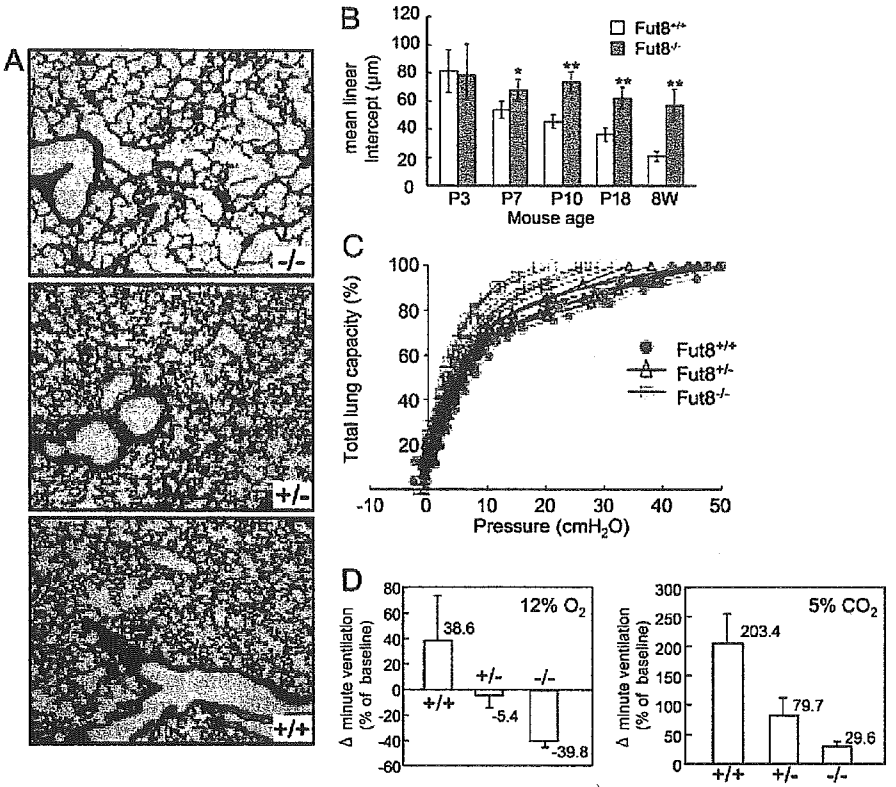

Fig. 2. Emphysematous change and impaired ventilatory response in *Fut8*$^{-/-}$ lung. (*A*) Representative histological sections (hematoxylin/eosin staining) of the lung of 18-day-old *Fut8*$^{+/+}$ (+/+), *Fut8*$^{+/-}$ (+/−), and *Fut8*$^{-/-}$ (−/−) pups show enlarged alveoli indicative of emphysema in *Fut8*$^{-/-}$ mice. (*B*) Lung morphometry at different stages. The mean linear intercepts of pulmonary alveoli were calculated at postnatal 3-, 7-, 10-, 18-day-old and 8-week-old mice. The diameters of the pulmonary alveoli were shown as the mean ± SD from three independent experiments. Statistical analysis was performed by using Student's *t* test. *, $P < 0.01$; **, $P < 0.001$ (versus the matched age of *Fut8*$^{+/+}$ mice). P, postnatal. (*C*) Lung compliance test. Static pressure–volume curves were plotted by using 19- to 20-day-old *Fut8*$^{-/-}$ (brown), *Fut8*$^{+/+}$ (pink), and *Fut8*$^{+/-}$ (blue) pups. (*D*) Comparison of changes in respiratory minute volume in response to hypoxic or hypercapnic air in conscious 19- to 20-day-old littermate *Fut8*$^{+/+}$ (+/+), *Fut8*$^{+/-}$ (+/−), and *Fut8*$^{-/-}$ (−/−) mice.

fucosylation affects MMP proteolytic function, because some MMPs such as MMP-9 contain *N*-glycans with core fucose. Taken together, these results suggest that overexpression of a set of MMPs might be causally linked to the development of emphysema in *Fut8*$^{-/-}$ mice.

To gain insight into the mechanism of induction of these MMPs in *Fut8*$^{-/-}$ mice, we established embryonic fibroblasts from *Fut8*$^{+/+}$ and *Fut8*$^{-/-}$ mice. Consistent with the data from the lungs shown in Fig. 3*A*, under resting conditions, McolB mRNA transcripts (Fig. 3*B*) and MMP-12 (Fig. 3*C*) and MMP-13 (data not shown) proteins secreted into the media were barely detected in wild-type embryonic fibroblasts, whereas they were clearly detected in *Fut8*$^{-/-}$ cells. To examine whether these changes in MMP expression levels were also manifested in the respective MMP proteolytic activities, gelatin and casein zymographies were performed by using the conditioned media from these embryonic cells. A differential band of ≈45 kDa, likely corresponding to the gelatinolytic activity of MMP-12, was observed in the gelatin zymogram of *Fut8*$^{-/-}$ cells. Likewise, a band of ≈55 kDa was detected in the casein zymogram of *Fut8* $^{-/-}$ cells (Fig. 6 *D* and *E*). In fact, the increased expression levels of both MMP-12 and MMP-13 secreted into media in the *Fut8*$^{-/-}$ cells were also confirmed by a Western blot (Fig. 6*F*). Consistent with these results, the enhancement of MMP-12 expression was also observed in lung tissues of *Fut8* $^{-/-}$ mice (Fig. 6*G*). These results demonstrate that the increased RNA and protein expression levels of some MMPs are accompanied by an increase in the proteolytic potential of cells from *Fut8*-deficient mice.

Lack of Core Fucose in TGF-β Receptor Leads to Inhibiting Its Function. Recently, it became clear that modification by N-glycosylation can affect the biological functions of many glycoprotein receptors. As described above, we found that loss of core fucosylation resulted in down-regulation of several receptor-mediated signaling pathways, such as TGF-β1 receptor, EGF receptor, and integrins, which are responsible for cell growth and differentiation, and also emphysema. The TGF-β1 receptor-mediated signaling pathway is a key pathway for regulating expression of ECM proteins, including suppression of MMPs to produce a "synthetic" phenotype (29). When the embryonic fibroblasts were treated with IL-1β, which enhances MMP expression, McolB mRNA levels were elevated markedly in both *Fut8*$^{+/+}$ cells and *Fut8*$^{-/-}$ cells (Fig. 3*B*). The enhancement of McolB expression stimulated by IL-1β was blocked by TGF-β1 treatment in *Fut8*$^{+/+}$ cells but not in *Fut8*$^{-/-}$ cells (Fig. 3*B*), indicating that the deletion of *Fut8* does not alter IL-1β-receptor-mediated function but diminishes TGF-β1-mediated signaling. The decreased response of TGF-β1 stimulation was also observed in protein expression levels of MMP-12 secreted into the media (Fig. 3*C*). To examine how core fucose affects TGF-β1-mediated signaling, we measured the binding activity of TGF-β1 for its surface receptor. The binding ability of ^{125}I-TGF-β1 was reduced significantly in *Fut8*$^{-/-}$ cells compared with *Fut8*$^{+/+}$ cells, which could be rescued by reintroducing *Fut8* to *Fut8*$^{-/-}$ cells (Fig. 3*D*). Consistent with this, the amount of TGF-β1 bound and cross-linked to type I, II, and III receptors was suppressed dramatically in *Fut8*$^{-/-}$ cells; these features were recovered by reintroducing *Fut8* to *Fut8*$^{-/-}$ cells (Fig. 3*E*). Actually, the levels of core fucosylation

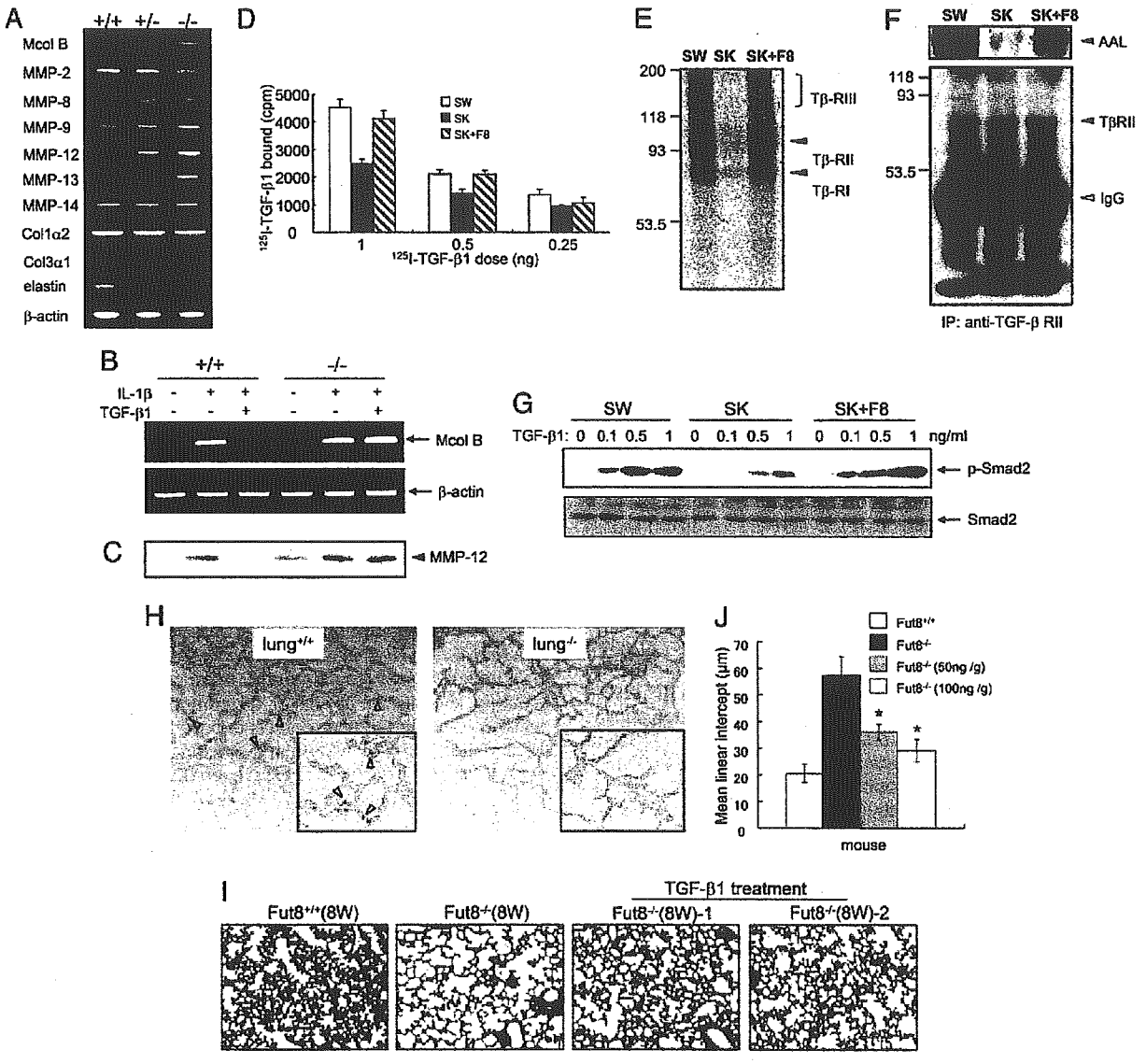

Fig. 3. Enhancement of some MMPs expression through down-regulation of TGF-β-receptor-mediated signaling in *Fut8*$^{-/-}$ lung and embryonic fibroblasts. (*A*) RT-PCR analysis of emphysema-relating genes (see Table 1, which is published as supporting information on the PNAS web site). Total RNAs from 18-day-old *Fut8*$^{+/+}$ (+/+), *Fut8*$^{+/-}$ (+/−), and *Fut8*$^{-/-}$ (−/−) lungs were used as template. β-Actin RNA is shown as a loading control. (*B*) Effects of IL-1β and TGF-β1 on McolB expression. These fibroblasts were preincubated with or without TGF-β1 (1 ng/ml) for 3 h and then further incubated with or without IL-1β (2 ng/ml) for 24 h. Total RNA was isolated and used as template. (*C*) Effects of IL-1β and TGF-β on protein expression of MMP-12 secreted into culture media. These fibroblasts were incubated with or without IL-1β and TGF-β1 in the absence of FCS. After incubation for 24 h, the conditioned media were concentrated and subjected to electrophoresis for Western blot. (*D*) Binding of ^{125}I-TGF-β1 to its receptors on the cell surface. These cells from *Fut8*$^{+/+}$ (+/+) and *Fut8*$^{-/-}$ (−/−) primary fibroblasts immortalized with SV40 large T, SW, and SK, respectively, or SK restored with *Fut8* (SK+F8), were incubated with different amounts of radiolabeled TGF-β1 as indicated and 10 ng of cold TGF-β1 for 2 h on ice. Cell lysate radioactivity was measured. (*E*) ^{125}I-TGF-β1 was bound and cross-linked to its receptors on cell surface. The cultured cells were incubated with 250 pM ^{125}I-TGF-β1 for 2 h at 4°C, and then cross-linked with reagent BS^3. (*F*) Analysis of fucosylation levels on TGF-β receptor II. TGF-β1 receptor II was immunoprecipitated from whole-cell lysates and then subjected to electrophoresis on 8% SDS/PAGE. After electroblotting, blots were probed by ALL lectin (*Upper*) and anti-TGF-β receptor II (*Lower*). (*G*) Effects of phosphorylated Smad2 levels on TGF-β1 stimulation. Serum-starved cells were treated with or without TGF-β1 at the indicated concentrations for 5 min and solubilized in lysis buffer as described in *Materials and Methods*. The cell lysates were detected by immunoblotting of anti-phospho-Smad2 antibody (*Upper*) and anti-Smad2 antibody (*Lower*). (*H*) The lung sections of 4-day-old mice were pretreated with hydroxygen blocking for 10 min at 37°C and then incubated with rabbit anti-human P-Smad2 antibody for 16 h at 4°C. The arrowheads indicate positive staining in *Fut8*$^{+/+}$ lung. (*I*) Therapeutic administration of recombinant TGF-β1 rescues emphysema-like changes in *Fut8*$^{-/-}$ mice. The surviving postnatal 18-day-old *Fut8*$^{-/-}$ mice were treated with or without recombinant TGF-β1 (50 or 100 ng/g of mouse body weight) for 20 times of injection every 2 days, and then the lung sections were subjected to hematoxylin/eosin staining. (*J*) Quantitative analyses of the pulmonary alveolar sizes were performed by mean linear intercept as described above. The diameters of the pulmonary alveoli were shown as the mean ± SD from three independent experiments. Statistical analysis was performed by using Student's *t* test. *, $P < 0.01$ (*Fut8*$^{-/-}$ mice treated with TGF-β versus the matched age of mice without treatment).

detected by AAL lectin in the TGF-β type II receptor, which is the primary binding subunit for TGF-β1 (30–32), were abolished in *Fut8*$^{-/-}$ cells, whereas they were recovered by restoring *Fut8* (Fig. 3*F*). The TGF-β1 signaling via receptors to intracellular mediators of the Smad family was suppressed significantly in *Fut8*$^{-/-}$ cells (Fig. 3*G*). Smad2 is a direct substrate for the activated TGF-β type